Conformational changes in tyrosine 11 of neurotensin are required to activate the neurotensin receptor 1

Fabian Bumbak[‡,†,§], Trayder Thomas[‼], Billy J. Noonan-Williams[‼], Tasneem M. Vaid[†,§,‡], Fei Yan[†,§], Alice R. Whitehead[‡], Shoni Bruell[‡], Martina Kocan[‡], Xuan Tan[•], Margaret A. Johnson[•], Ross A. D. Bathgate[‡,†], David K. Chalmers[‼,], Paul R. Gooley[†,§,*], and Daniel J. Scott[‡,†,*].*

SUPPORTING INFORMATION

TABLE OF CONTENTS

	Item	Page
1	Figure S1	S-3
2	Figure S2	S-4
3	Figure S3	S-5
4	Table S1	S-6
5	Figure S4	S-7
6	Table S2	S-8
7	Table S3	S-9
8	Figure S5	S-10
9	Table S4	S-11
10	Table S5	S-12
11	Table S6	S-12
12	Figure S6	S-13
13	Figure S7	S-14
14	Table S7	S-15
15	Table S8	S-16
16	Table S9	S-17
17	Table S10	S-19
18	Table S11	S-21
19	Figure S8	S-22
20	Figure S9	S-23
21	Table S12	S-24
22	Figure S10	S-26
23	Figure S11	S-27
24	Figure S12	S-28
25	Figure S13	S-29
26	Figure S14	S-30
27	Supporting information	S-31
28	Figure S15	S-33
29	Figure S16	S-34
30	Figure S17	S-35
31	References	S-36

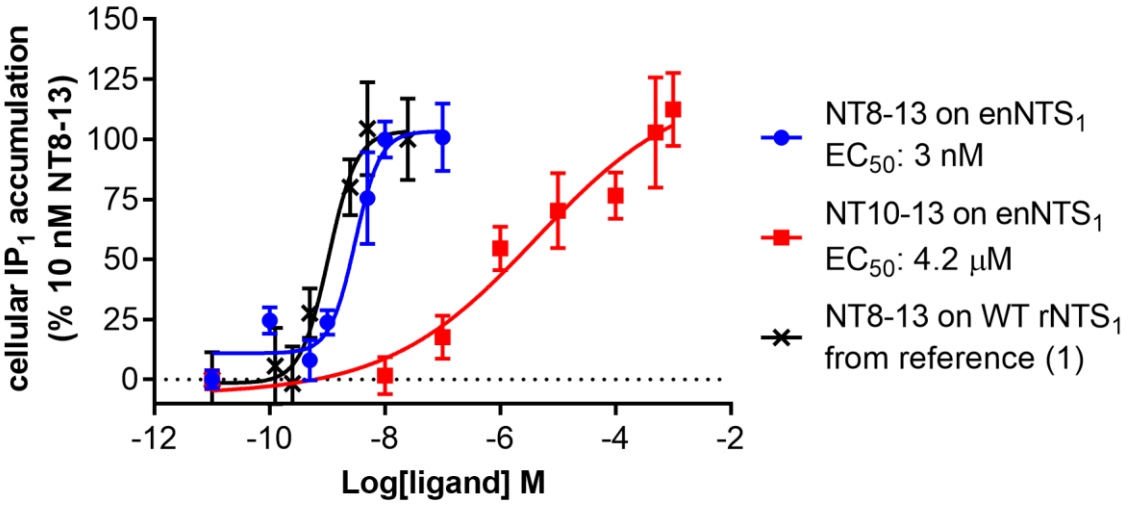

Figure S1. IP_1 dose response curves at HEK 293T cells expressing $enNTS_1$. Values for NT8-13 and NT10-13 on $enNTS_1$ shown in blue discs and red squares respectively. Data are the mean (± SE) of two experiments done in triplicate. Data were fitted using a variable Hill slope equation in Graphpad Prism. Data for NT8-13 induced stimulation of IP_1 accumulation in wild-type (WT) $rNTS_1$ expressing cells taken from Bumbak *et al.*, 2018[1], are indicated with black crosses for comparison.

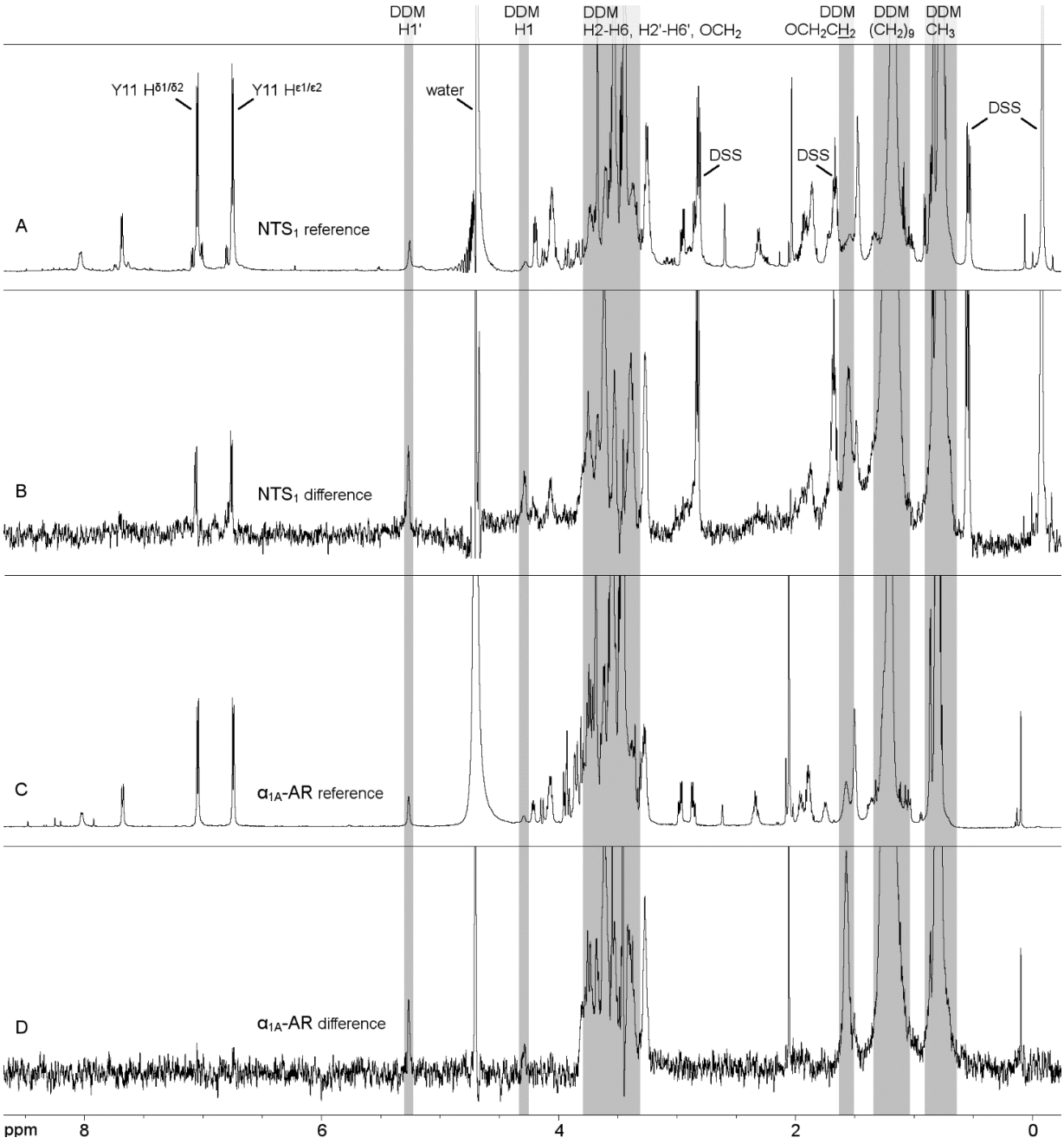

Figure S2. Reference and difference spectra of NT10-13 against enNTS$_1$ and α$_{1A}$-AR. A) Reference 1D NMR spectrum of NT10-13 against enNTS$_1$. B) STD NMR (difference) spectrum of NT10-13 against enNTS$_1$. C) Reference 1D NMR spectrum of NT10-13 against α$_{1A}$-AR. D) STD NMR (difference) spectrum of NT10-13 against α$_{1A}$-AR. All spectra were recorded using 512 scans with selective saturation at -1 ppm. The samples contained 5 µM of cleaved receptor and 500 µM of NT10-13 in 50 mM potassium phosphate, 100 mM NaCl, 400 µM DDM, pH 7.4. The enNTS$_1$ sample contained 500 µM DSS as reference which was omitted from the α$_{1A}$-AR sample (and further experiments) due to interference of DSS resonances with NT10-13 resonances. The STD effect by DSS is due to non-specific interactions as observed in samples without receptor.

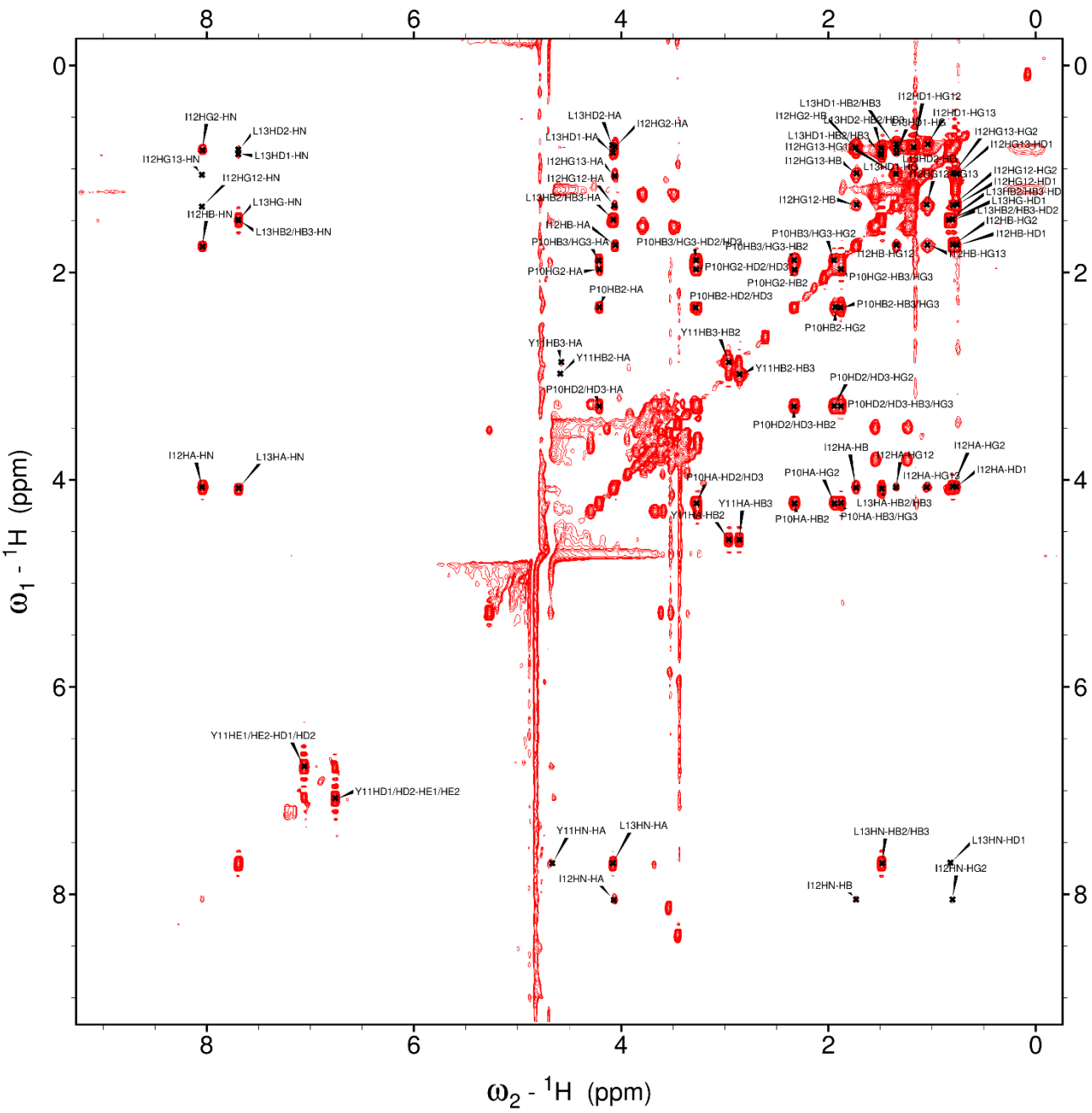

Figure S3. 2D ^{1}H-^{1}H TOCSY spectrum of NT10-13. The spectrum was recorded under the same conditions as STD NMR experiments (5 µM cleaved enNTS$_1$ and 500 µM NT10-13 in 50 mM potassium phosphate buffer, 100 mM NaCl, 0.02% DDM (400 µM), 10% D_2O, pH 7.4)

Table S1. NT10-13 chemical shift assignment. 2D ^{1}H-^{1}H TOCSY-based chemical shift assignment of NT10-13 protons. Resonances have not been stereoassigned, except for P10 $H^{\beta 2}$ (2.33 ppm) and P10 $H^{\beta 3}$ (1.89 ppm).

Residue	NH	H^{α}	H^{β}	others
P10	-	4.22	2.33/1.89	$H^{\gamma 2/\gamma 3}$ 1.95/1.89; $H^{\delta 2/\delta 3}$ 3.28/3.26
Y11	7.69	4.58	2.94/2.86	$H^{\delta 1/\delta 2}$ 7.06; $H^{\varepsilon 1/\varepsilon 2}$ 6.77
I12	8.05	4.07	1.73	$H^{\gamma 12/\gamma 13}$ 1.34/1.04; $H^{\gamma 2}$ 0.80; H^{δ} 0.76
L13	7.69	4.08	1.45	H^{γ} 1.45; $H^{\delta 1/\delta 2}$ 0.83/0.80

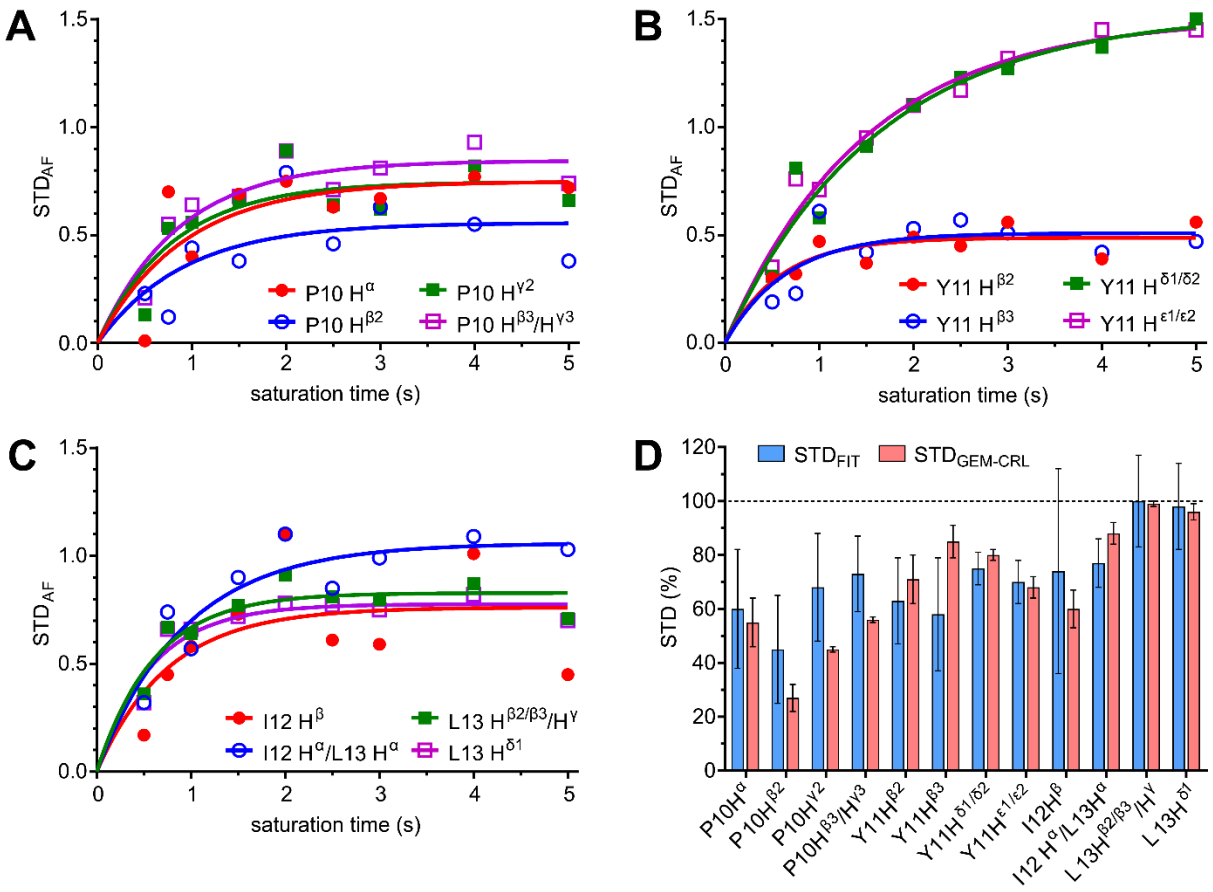

Figure S4. STD epitope mapping. STD build-up curves for A) P10, B) Y11 and C) I12 and L13 protons generated from STD_{AF} values acquired with increasing saturation times and selective saturation at 10 ppm. D) Comparison of initial slopes at 0 s saturation time (STD_{FIT}, grey bars) extracted from exponential fits of build-up curves with T_1 corrected amplification factors ($STD_{GEM\text{-}CRL}$, light blue bars) at 10 ppm selective saturation and 3 s saturation time. The error bars for STD_{FIT} represent the standard error of the mean from exponential fitting. $STD_{GEM\text{-}CRL}$ represent the mean values from four independent experiments (± SE). Overlapping resonances P10 $H^{\beta3}/H^{\gamma3}$, I12 H^{α}/L13 H^{α} and L13 $H^{\beta2/\beta3}/H^{\gamma}$ were treated as bulk signals.

Table S2. STD enhancements derived from exponential curve fitting of build-up curves. T_1 relaxation times were determined for each proton using the inversion recovery method. STD_{Max} (± SE) values were derived from exponential fits of experimentally determined STD_{AF} values. STD_{Max} [%] are the STD_{Max} values normalised relative to the largest value. STD_{Max}/T_1 [s^{-1}] are the T_1 corrected STD_{Max} values. STD_{FIT} represent the initial fits at 0 s saturation of build-up curves derived from exponential line fitting (± SE). STD_{FIT} [%] are the STD_{FIT} [s^{-1}] values normalised relative to the largest value.

proton	T_1 [s]	STD_{Max}	STD_{Max} [%]	STD_{Max}/T_1 [s^{-1}]	STD_{Max}/T_1 [%]	STD_{FIT} [s^{-1}]	STD_{FIT} [%]
P10 H^{α}	0.82	0.75 ± 0.11	49	0.91 ± 0.13	65	0.82 ± 0.30	60
P10 $H^{\beta2}$	1.14	0.56 ± 0.10	37	0.49 ± 0.09	35	0.61 ± 0.28	45
P10 $H^{\gamma2}$	1.05	0.75 ± 0.08	49	0.71 ± 0.07	51	0.93 ± 0.27	68
P10 $H^{\beta3}/H^{\gamma3}$	1.05	0.84 ± 0.06	56	0.80 ± 0.06	57	0.98 ± 0.20	73
Y11 $H^{\beta2}$	0.47	0.49 ± 0.03	32	1.04 ± 0.07	74	0.85 ± 0.22	63
Y11 $H^{\beta3}$	0.46	0.51 ± 0.06	33	1.11 ± 0.12	79	0.78 ± 0.28	58
Y11 $H^{\delta1/\delta2}$	1.33	1.51 ± 0.07	98	1.13 ± 0.05	81	1.02 ± 0.08	75
Y11 $H^{\varepsilon1/\varepsilon2}$	1.62	1.53 ± 0.12	100	0.95 ± 0.07	67	0.95 ± 0.11	70
I12 H^{β}	0.78	0.76 ± 0.13	50	0.98 ± 0.17	70	1.01 ± 0.52	74
I12 H^{α}/L13 H^{α}	0.90	1.10 ± 0.05	72	1.21 ± 0.06	87	1.04 ± 0.12	77
L13 $H^{\beta2/\beta3}/H^{\gamma}$	0.59	0.83 ± 0.04	54	1.40 ± 0.07	100	1.36 ± 0.24	100
L13 $H^{\delta1}$	0.64	0.78 ± 0.03	51	1.21 ± 0.05	86	1.33 ± 0.22	98

Table S3. T_1 corrected $STD_{GEM-CRL}$ values. Absolute and relative $STD_{GEM-CRL}$ values given for 4 independent experiments with selective saturation at 10ppm. The average was calculated for the relative $STD_{GEM-CRL}$ values only (± SE).

Proton	$STD_{GEM-CRL}$				$STD_{GEM-CRL}$ (%)				**average (%)**
	1	2	3	4	1	2	3	4	
P10 H^{α}	0.86	1.29	1.25	0.39	63	55	62	29	**55 ± 9**
P10 $H^{\beta 2}$	0.57	0.40	0.43	0.32	42	20	21	23	**27 ± 5**
P10 $H^{\gamma 2}$	0.60	0.96	0.90	0.59	44	48	45	43	**45 ± 1**
P10 $H^{\beta 3}/H^{\gamma 3}$	0.79	1.14	1.13	0.72	58	57	56	53	**56 ± 1**
Y11 $H^{\beta 2}$	1.21	0.95	1.35	1.12	89	48	67	82	**71 ± 9**
Y11 $H^{\beta 3}$	1.13	1.99	1.46	1.19	83	100	72	87	**85 ± 6**
Y11 $H^{\delta 1/\delta 2}$	1.14	1.58	1.54	1.10	84	79	76	80	**80 ± 2**
Y11 $H^{\varepsilon 1/\varepsilon 2}$	0.93	1.34	1.20	1.08	69	67	59	79	**68 ± 4**
I12 H^{β}	0.78	1.60	1.07	0.68	57	80	53	50	**60 ± 7**
I12 H^{α}/L13 H^{α}	1.17	1.90	1.88	1.04	86	96	93	76	**88 ± 4**
L13 $H^{\beta 2/\beta 3}/H^{\gamma}$	1.36	1.93	2	1.37	100	97	99	100	**99 ± 5**
L13 $H^{\delta 1}$	1.19	1.98	2.03	1.31	87	99	100	95	**96 ± 3**

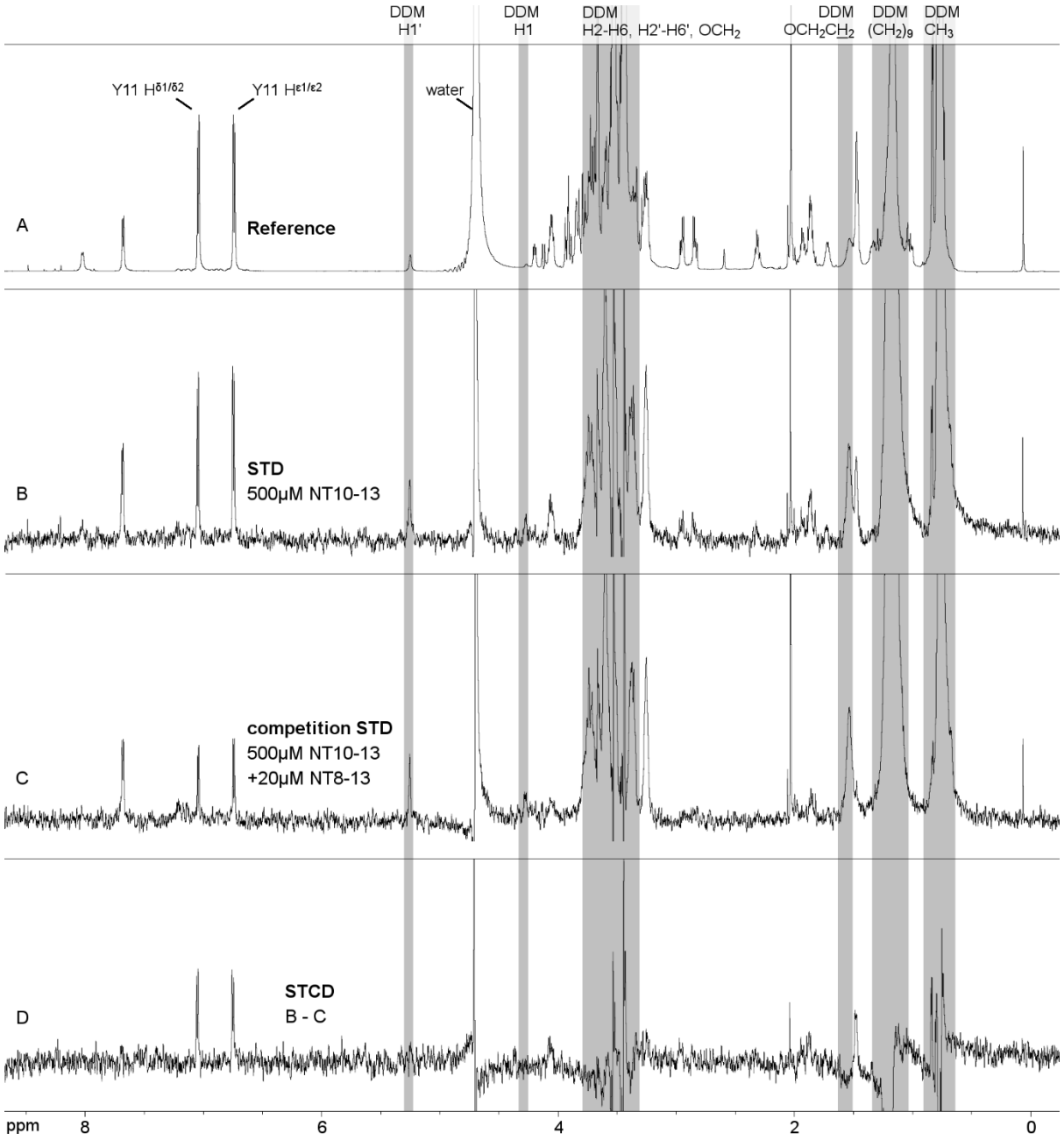

Figure S5. The STCD experiment. A) Reference 1D NMR spectrum. B) STD NMR spectrum. C) Competition STD NMR spectrum. D) The STCD (Saturation Transfer Competition Difference) spectrum was obtained by subtracting spectrum C from spectrum B. All spectra were recorded using 2048 scans with selective saturation at 10 ppm. The samples contained 5 µM enNTS$_1$ and 500 µM NT10-13 in 50 mM potassium phosphate, 100 mM NaCl, 400 µM DDM, pH 7.4. 20 µM NT8-13 (competitor) was added to sample C to fully saturate the orthosteric binding site at enNTS$_1$.

Table S4. Remaining signal intensities after competition double difference treatment. Fractions of remaining signal intensities were normalised relative to the respective signals in STD spectra prior to STCD subtraction. Protons are listed including their chemical shifts (in ppm).

Proton (ppm)	% of STD
P10 H^{α} (4.22)	< 0
P10 $H^{\beta 2}$ (2.33)	59
P10 $H^{\gamma 2}$ (1.95)	61
P10 $H^{\beta 3}/H^{\gamma 3}$ (1.89)	51
Y11 $H^{\beta 2}$ (2.94)	76
Y11 $H^{\beta 3}$ (2.86)	60
Y11 $H^{\delta 1/\delta 2}$ (7.06)	53
Y11 $H^{\varepsilon 1/\varepsilon 2}$ (6.77)	54
I12 H^{β} (1.73)	33
I12 H^{α}/L13 H^{α} (4.07)	35
L13 $H^{\beta 2/\beta 3}/H^{\gamma}$ (1.45)	54
L13 $H^{\delta 1}$ (0.83)	41

Table S5. enNTS$_1$ MD trajectory RMSDs. The root mean square deviations (RMSDs) calculated for each trajectory based on reduced versions of the trajectories (1 frame per ns, waters removed) considering the C^{α} atoms of residues L66 – T88 (TM1), R101 – N127 (TM2), G138 – I171 (TM3), 187 – 208 (TM4), 231 – 263 (TM5), 302 – 332 (TM6) and 340 – 372 (TM7). Trajectory alignment was carried out based on the same atoms used for RMSD calculations.

trajectory	length	RMSD (Å)			
	μs	average	SD	min	max
NT8-13 enNTS$_1$					
1	3.251	1.587	0.338	0.552	2.860
2	2.359	1.509	0.337	0.564	2.731
3	2.371	1.328	0.263	0.563	2.721
4	2.341	1.345	0.318	0.545	3.073
NT10-13 enNTS$_1$					
1	2.375	1.661	0.516	0.539	3.196
2	2.367	1.215	0.230	0.562	2.522
3	2.363	1.562	0.377	0.574	3.112
4	2.378	1.282	0.241	0.538	2.907

Table S6. Distribution of MD simulations across discrete clusters based on φ, ψ and χ1 dihedral angles. Clustering over all four MD trajectories available for each receptor-peptide complex was carried out using MSMBuilder 3.3.0[2]. The k-means method[3] was used to generate 10 clusters by comparing ϕ, ψ and χ1 dihedral angle distributions.

cluster	frames per cluster	
	NT8-13	NT10-13
1	1164	1225
2	431	627
3	771	686
4	1208	1013
5	877	663
6	771	1613
7	1144	568
8	1236	1739
9	1895	783
10	881	562
total frames	10318	9479

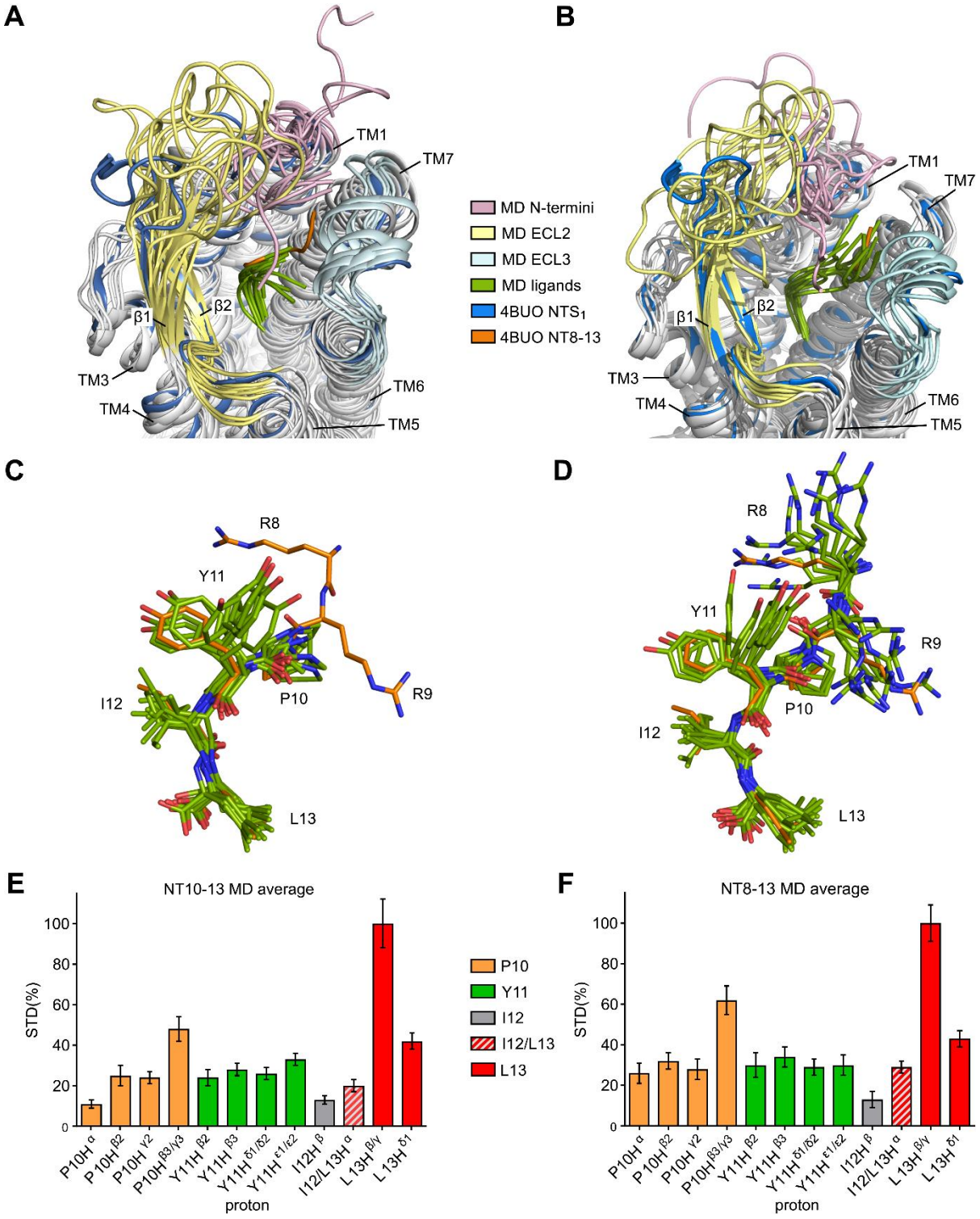

Figure S6. Cluster analysis of NT10-13 and NT8-13 MD simulations. Superimpositions of the 10 MD cluster representatives of (A) NT10-13 and (B) NT8-13 bound enNTS$_1$ showing increased dynamics for ECL2 (pale yellow) and the receptor N-terminus (pink) as well as an inward shift of ECL3 (pale cyan) when compared to the crystal structure of NTS$_1$ (PDB 4BUO, shown in blue). NT10-13 and NT8-13 from MD clusters are shown in green, and NT8-13 as observed in the crystal structure is shown in orange for comparison. The MD cluster frames were aligned using the C$^{\alpha}$ atoms of the receptor and peptide residues. C) and D) Superimposed MD cluster peptides NT10-13 and NT8-13 highlighting the dynamics of the Y11 side chain (green) including NT8-13 as observed in

the crystal structure (PDB 4BUO, shown orange). The peptides were aligned using the C^{α} atoms. E) Epitope map based on averaged STD enhancements of the 10 cluster representatives from the NT10-13 MD simulations normalized to the maximum value. The corresponding values (± SE) are P10 H^{α} 11 ± 2 %, P10 $H^{\beta 2}$ 25 ± 5 %, P10 $H^{\gamma 2}$ 24 ± 3 %, P10 $H^{\beta 3/\gamma 3}$ 48 ± 6 %, Y11 $H^{\beta 2}$ 24 ± 4 %, Y11 $H^{\beta 3}$ 28 ± 3 %, Y11 $H^{\delta 1/\delta 2}$ 26 ± 3 %, Y11 $H^{\varepsilon 1/\varepsilon 2}$ 33 ± 3 %, I12 H^{β} 13 ± 2 %, I12 H^{α}/L13 H^{α} 20 ± 3 %, L13 $H^{\beta 2/\beta 3}$/H^{γ} 100 ± 12 % and L13 $H^{\delta 1}$ 42 ± 4 %. F) Epitope map based on averaged STD enhancements of the 10 cluster representatives from the NT8-13 MD simulations normalized to the maximum value. The corresponding values (± SE) are P10 H^{α} 26 ± 5 %, P10 $H^{\beta 2}$ 32 ± 4 %, P10 $H^{\gamma 2}$ 28 ± 5 %, P10 $H^{\beta 3/\gamma 3}$ 62 ± 7 %, Y11 $H^{\beta 2}$ 30 ± 6 %, Y11 $H^{\beta 3}$ 34 ± 5 %, Y11 $H^{\delta 1/\delta 2}$ 29 ± 4 %, Y11 $H^{\varepsilon 1/\varepsilon 2}$ 30 ± 5 %, I12 H^{β} 13 ± 4 %, I12 H^{α}/L13 H^{α} 29 ± 3 %, L13 $H^{\beta 2/\beta 3}$/H^{γ} 100 ± 9 % and L13 $H^{\delta 1}$ 43 ± 4 %.

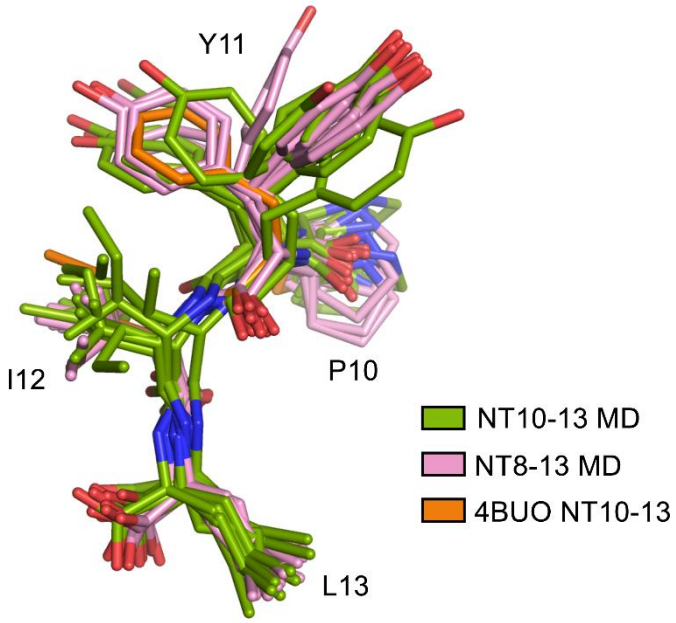

Figure S7. Comparison of NT10-13 and NT8-13 peptides from MD cluster frames. Superimposition of exposed views of NT10-13 (green) and NT8-13 (pink) peptides. The peptide (residues 10-13) observed in the crystal structure (PDB 4BUO, orange) was included for comparison. Residues R8 and R9 from NT8-13 MD cluster frames and PDB 4BUO were omitted for simplicity.

Table S7. Peptide torsion angles in NT10-13 MD cluster frames. Torsion angles (in degrees) were measured using WhatIF[4] for peptides only as observed in frames representing the centre of each NT10-13 MD cluster. The φ angle was not determined for the N-terminal residue P10 while the ψ and ω angles were not determined for the C-terminal residue L13.

residue	angle	Frame 1	Frame 2	Frame 3	Frame 4	Frame 5	Frame 6	Frame 7	Frame 8	Frame 9	Frame 10
P10	ψ	160.5	149.2	119.3	151.0	159.0	131.4	165.8	157.3	162.6	154.2
	ω	-179.2	-173.5	167.1	-172.8	161.6	-172.8	-168.7	-168.4	-169.5	175.3
Y11	φ	-113.1	-133.9	-121.2	-93.8	-74.7	-115.4	-99.4	-147.5	-124.9	-108.1
	ψ	-45.1	-35.4	-44.0	152.1	152.0	168.1	-65.5	-33.0	-12.2	161.5
	ω	176.5	165.6	-174.1	-171.1	176.8	178.9	-159.7	-178.5	-176.6	-175.7
	χ_1	-90.3	54.4	68.2	-61.8	-136.8	47.6	46.0	-88.3	-77.1	-79.1
	χ_2	-91.1	88.1	-62.8	-64.9	-83.5	-80.7	-68.4	88.6	93.7	76.0
I12	φ	-66.3	-94.7	-77.7	50.1	56.3	63.6	-73.7	-90.3	-79.4	61.5
	ψ	145.3	137.7	114.2	91.6	124.5	114.2	129.7	136.1	124.2	97.0
	ω	-175.8	-178.3	158.1	175.9	-175.2	178.1	167.2	179.0	178.6	177.0
	χ_1	63.3	-153.4	52.9	-2.6	63.6	64.4	31.2	-55.4	52.0	-55.5
	χ_2	-163.3	69.2	169.6	108.5	160.9	177.4	159.5	-48.7	149.0	146.3
L13	φ	-116.8	-63.5	-86.8	-65.0	-104.4	-79.1	-85.0	-99.3	-134.0	-84.5
	χ_1	-170.1	-81.9	-157.5	-170.8	-169.1	-163.7	-113.7	-168.3	-109.7	-175.6
	χ_2	58.2	-170.8	72.7	56.5	61.8	58.3	159.5	72.2	166.9	83.2

Table S8. Peptide torsion angles in NT8-13 MD cluster frames. Torsion angles (in degrees) were measured using WhatIF[4] for peptides only as observed in frames representing the centre of each NT8-13 MD cluster. The φ angle was not determined for the N-terminal residue R8 while the ψ and ω angles were not determined for the C-terminal residue L13.

residue	angle	4BUO	Frame 1	Frame 2	Frame 3	Frame 4	Frame 5	Frame 6	Frame 7	Frame 8	Frame 9	Frame 10
R8	ψ	172.3	145.4	156.2	131.4	131.9	146.2	160.5	135.6	158.4	173.5	147.3
	ω	-177.4	-175.5	168.9	173.7	-179.7	175.2	-167.5	173.8	-179.5	177.1	163
	χ_1	57.1	-158	-67.7	-172	-173.4	-61.2	-64.4	-68.3	-83.9	-61.8	-54.9
	χ_2	178.9	168.7	176.5	-174.8	83.7	168	-153.2	-145.1	178.7	166	168.4
	χ_3	178.9	73.7	168.5	-172.9	-171.1	-148.9	164	74.2	-148.7	-78.5	-174.8
	χ_4	178.5	133.9	-100.9	167.1	-114.2	-159.9	-83.4	-121.8	179.2	-111.6	107.6
	χ_5	0.1	-13.6	-1.8	-20.1	4.7	-7.4	16.1	2.4	-10	-3.2	5
R9	φ	-124.4	-119.6	-69.1	-106	-109.2	-66.2	-113.7	-74	-55	-63.6	-60.4
	ψ	137.4	132.2	153.8	137.7	100.4	147.6	137.6	140.7	140.2	145.3	138
	ω	177.7	176.3	145.6	175.6	169.4	161.3	172.7	178.2	160.6	168.2	174.6
	χ_1	-167.4	-75.2	-111.6	-87.5	-167.4	-155.9	-74.1	-170.5	-64.7	-81.9	-85.5
	χ_2	-172.5	167	177.9	-167.3	69.3	176.7	-153.9	-171.7	-168.5	175.6	-173
	χ_3	-168.3	61.5	61.5	-56.1	162.8	69.1	84	68.1	-79.3	-171.4	178.9
	χ_4	94.9	-148.2	-127.1	-166	70.4	-163.5	56.2	166.4	159.7	111.8	-149.1
	χ_5	0.1	10.5	8.2	-4.9	-4.7	-16.9	5.2	-10.3	-3.6	-8.5	-4.8
P10	φ	-57.5	-65.8	-66.9	-71.5	-72.7	-66.9	-64.6	-67.4	-50.7	-55.7	-84.9
	ψ	147.3	158.9	165.8	-16.8	153.6	162.3	-28.8	164	177	154	-10.9
	ω	178.6	-177.7	176.9	-177.9	-167.9	176.7	-174.7	-163.1	-166.5	-171.4	171.7
Y11	φ	-114.1	-104.5	-115.9	65.8	-129.5	-80.2	58.4	-91.9	-103.6	-106	66.6
	ψ	-6.3	-41	-13.3	-76.9	-63.2	-44.6	-61.9	-43.7	-40.3	-63.4	-70.2
	ω	-179.5	-174.1	179	-173.9	175.2	-171	-179.4	178.1	-178	176.8	-172.2
	χ_1	54	28	65.9	-78.6	41.9	-86.8	-77	56	-92.6	-57.8	-68.6
	χ_2	90	-57.4	69.7	-82.1	-79.8	52.9	-86.3	68.8	70.1	66.6	-76.7
I12	φ	-96.4	-88.5	-105.5	-73.5	-58.9	-90.9	-86.4	-80.1	-70.3	-74.3	-81.6
	ψ	115	147.2	132.6	155.7	113.3	137.7	122.5	160.3	155.5	137.9	149.5
	ω	178.3	-179.8	-176.5	-171.9	170	175.8	-177.2	173.9	-174.6	-167.5	-179.8
	χ_1	-62.9	-156.2	64.2	27.4	63.1	56.5	65.9	66.3	59.7	44.7	-169.3
	χ_2	-179.8	80.3	162.5	72.4	170.1	173.8	170.2	-179.6	162.2	165.9	52.3
L13	φ	-92.9	-116.8	-87.3	-153	-101.8	-106.7	-85.7	-166	-130.8	-121.5	-147.7
	χ_1	-179.3	-174.6	-149	-162.4	-177.3	-156.6	-164.6	-169.3	-152.3	-172	-167.5
	χ_2	60.5	50.1	74.6	53	117.1	66.9	73.6	71.1	60.2	68.5	75.9

Table S9. Hydrogen bonds between NT8-13 and published NTS_1 crystal structures. Structures 1-4 correspond to crystal structures with PDB access codes 4BWB (NTS_1-H4), 3ZEV (NTS_1 TM86V-ΔIC3A), 4BUO (NTS_1 TM86V-ΔIC3B) and 4BV0 (NTS1-OGG7-ΔIC3A)[5]. Structure 5 corresponds to PDB access code 4GRV (NTS_1 GW5-T4L)[6]. Structures 6 and 7 correspond to PDB access codes 4XXE (NTS_1 ELF-T4L) and 4XES (NTS_1 LF-T4L) respectively[7]. Gly residues marked with * represent non-native residues at the N-terminus of NT8-13 resulting from proteolytic cleavage from a ligand column. Ligand residues not observed in the corresponding crystal structures/chains are marked "n.a". Hydrogen bond analysis was carried out using the PDBePISA server (http://www.ebi.ac.uk/pdbe/pisa/).

Ligand atom	Distance (Å) in structure (chain)											NTS_1 atom	Location in NTS_1
	1 (A)	1 (B)	2 (A)	2 (B)	3 (A)	3 (B)	4 (A)	4 (B)	5	6	7		
Hydrogen bonds													
G6 [N]*	n.a.	n.a	n.a.	3.4	n.a.	n.a.	n.a.	n.a.	n.a.	n.a.	n.a.	E337 [O]	ECL3
G7 [N]*	n.a.	n.a	-	-	n.a.	n.a.	3.88	-	n.a.	n.a.	n.a.	D336 [O]	ECL3
	n.a.	n.a	-	3.09	n.a.	n.a.	2.8	-	n.a.	n.a.	n.a.	W339 [O]	ECL3
R8 [N]	3.61	n.a.	-	-	-	-	-	-	-	-	-	D336 [O]	ECL3
	2.88	n.a.	-	-	-	-	-	3.73	-	-	-	W339 [O]	ECL3
R8 [NH1]	-	n.a.	3.32	-	-	-	-	-	-	-	-	S53 [O]	N
	-	n.a.	2.9	-	2.45	-	-	-	-	2.78	3.38	D54 [O]	N
	-	n.a.	3.02	-	-	-	-	-	3.89	2.65	2.73	D56 [O]	N
R8 [NH2]	2.36	n.a.	-	3.18	-	3.87	2.61	2.3	-	-	-	D54 [O]	N
	2.24	n.a.	-	2.56	2.9	2.26	2.63	3.89	-	-	-	D56 [O]	N
	-	n.a.	3.04	-	-	-	-	-	-	-	-	N58 [OD1]	N
	-	n.a.	-	-	-	-	-	-	-	-	3.67	T341 [OG1]	ECL3
R8 [NE]	-	n.a.	-	-	-	-	-	-	-	2.79	-	D54 [O]	N
R9 [NH1]	2.52	n.a.	-	-	-	2.84	-	2.71	-	2.4	2.91	F331 [O]	TM6
	-	n.a.	-	-	-	-	-	-	-	-	3.87	C332 [O]	ECL3
	-	n.a.	2.67	-	2.72	-	2.64	-	-	-	2.64	I334 [O]	ECL3
	-	n.a.	2.61	3.43	2.9	-	2.69	-	-	-	-	D336 [OD1]	ECL3
R9 [NH2]	-	n.a.	2.43	-	3.28	-	2.79	-	2.46	-	-	F331 [O]	TM6
	3.86	n.a.	-	-	-	-	3.07	-	-	-	-	V332 [O]	ECL3
	2.34	n.a.	-	2.21	-	2.64	-	2.36	-	3.01	-	I334 [O]	ECL3
	-	n.a.	-	-	-	-	-	2.45	-	-	3.07	D336 [OD1]	ECL3
R9 [NE]	2.94	n.a.	-	-	-	3.42	-	-	-	-	-	D336 [OD1]	ECL3
P10 [O]	-	-	-	-	-	-	-	-	3.86	-	-	R213 [NH1]	ECL2-β2
Y11 [OH]	2.27	2.48	2.58	2.86	2.51	2.55	2.7	3.24	2.54	2.8	2.8	L55 [O]	N
	3.88	-	-	3.25	3.35	3.5	3.58	3.26	-	-	-	H132 [O]	ECL1
	-	-	-	-	-	-	-	-	-	3.76	-	H133 [N]	ECL1
	-	3.49	-	-	-	-	3.82	-	-	-	-	H133 [ND1]	ECL1
Y11 [O]	3.02	3.1	2.88	2.91	2.96	2.9	-	-	2.81	2.74	-	T226 [OG1]	ECL2-β2
I12 [O]	3.15	3.03	2.91	3.17	2.58	2.88	2.64	2.66	3.11	2.6	2.89	Y347 [OH]	TM7
L13 [O]	n.a.	n.a.	2.97	-	2.9	-	3.2	-	-	-	-	Y146 [OH]	TM3
	n.a.	n.a.	3.86	-	-	-	3.75	-	-	-	-	Y351 [OH]	TM7
	n.a.	n.a.	-	3.23	-	2.99	-	2.64	-	3.12	2.83	R327 [NH1]	TM6
	n.a.	n.a.	-	3.03	-	3.38	-	2.7	2.41	3.19	-	R327 [NH2]	TM6
	n.a.	n.a.	-	-	-	-	-	-	-	2.82	-	R328 [NH1]	TM6
L13 [OXT]	n.a.	n.a.	-	2.7	-	2.97	-	2.92	2.61	2.73	2.56	Y146 [OH]	TM3
	n.a.	n.a.	-	-	-	-	-	-	-	3	-	Y351 [OH]	TM7
	n.a.	n.a.	2.91	-	2.81	-	2.42	-	-	-	-	R327 [NH1]	TM6
	n.a.	n.a.	3.17	-	3.08	-	-	-	-	-	-	R327 [NH2]	TM6

L13 [N]	n.a.	n.a.	3.61	-	3.86	3.88	3.83	-	3.58	-	-	Y146 [OH]	TM3
Salt bridges													
R9 [NH1]	-		2.61	3.43	2.9	-	2.69	-	-	-	-	D336 [OD1]	ECL3
R9 [NH2]	3.78	n.a.	-	3.07	-	-	-	2.45	-	-	3.07	D336 [OD1]	ECL3
R9 [NE]	2.94	n.a.	3.5	3.19	-	3.42	3.52	3.07	-	-	-	D336 [OD1]	ECL3
L13 [O]	n.a.	n.a.	-	3.23	-	2.99	3.97	2.64	2.97	3.12	-	R327 [NH1]	TM6
	n.a.	n.a.	-	3.03	-	3.38	-	2.7	2.41	3.19	-	R327 [NH2]	TM6
	n.a.	n.a.	-	-	-	-	-	-	-	2.82	-	R328 [NH1]	TM6
L13 [OXT]	n.a.	n.a.	2.91	-	2.81	-	2.42	-	-	-	-	R327 [NH1]	TM6
	n.a.	n.a.	3.17	-	3.08	-	3.53	-	-	-	-	R327 [NH2]	TM6

Table S10. Comparison of ligand/receptor hydrogen bond occupancies observed in NT8-13 and NT10-13 MD trajectories. Hydrogen bond occupancies were calculated using the "hbond" tool which is part of the MDTraj analysis software package[8] using the Baker-Hubbard criteria: 2.5 Å < hydrogen bond length < 4.0 Å; 120° < hydrogen bond angle < 180°. Only hydrogen bonds with at least 50% occupancy in either trajectory are listed.

Ligand atom	Coupled via	NTS_1 atom	Location in NTS_1	Hydrogen bond occupancy (%)							
				NT8-13 / $enNTS_1$ trajectories				NT10-13 / $enNTS_1$ trajectories			
				1	2	3	4	1	2	3	4
ARG 8 [NE]	ARG 8 [HE]	SER 53 [O]	N-term			63		only observed for NT8-13			
ARG 8 [NE]	ARG 8 [HE]	ASP 54 [O]	N-term		11	72					
ARG 8 [NE]	ARG 8 [HE]	ASP 54 [N]	N-term			62					
ARG 8 [NH2]	ARG 8 [HH21]	SER 53 [O]	N-term		11	65					
ARG 8 [NH2]	ARG 8 [HH21]	ASP 54 [O]	N-term			70					
ARG 8 [NH2]	ARG 8 [HH21]	LEU 55 [O]	N-term			54					
ARG 8 [NH2]	ARG 8 [HH21]	ASP 56 [N]	N-term			57					
ARG 9 [O]	ASP 54 [H]	ASP 54 [N]	N-term				100				
ARG 9 [N]	ARG 9 [H]	ASN 52 [O]	N-term				74				
ARG 9 [N]	ARG 9 [H]	ASP 54 [OD1]	N-term		77	57					
ARG 9 [N]	ARG 9 [H]	ASP 54 [OD2]	N-term		76	59					
ARG 9 [N]	ASP 54 [H]	ASP 54 [N]	N-term				65				
ARG 9 [N]	ARG 9 [H]	ASP 336 [OD1]	ECL3	83		15	94				
ARG 9 [N]	ARG 9 [H]	ASP 336 [OD2]	ECL3	83		16	93				
PRO 10 [O]	THR 226 [HG1]	THR 226 [OG1]	ECL2-β2			11			76	22	
PRO 10 [N]	PRO 10 [H]	ASP 54 [OD1]	N-term					98	96		
PRO 10 [N]	PRO 10 [H]	ASP 54 [OD2]	N-term					98	96		
PRO 10 [N]	PRO 10 [H]	ASP 336 [OD1]	ECL3							100	37
PRO 10 [N]	PRO 10 [H]	ASP 336 [OD2]	ECL3							99	37
TYR 11 [OH]	TYR 11 [HH]	LEU 55 [O]	N-term				80				
TYR 11 [OH]	TYR 11 [HH]	ASP 56 [OD1]	N-term			98					
TYR 11 [OH]	TYR 11 [HH]	ASP 56 [OD2]	N-term			99					
TYR 11 [OH]	TYR 11 [HH]	ASP 56 [N]	N-term			33	56				
TYR 11 [OH]	TYR 11 [HH]	HIS 132 [NE2]	ECL1			55			20		
TYR 11 [OH]	HIS 132 [HE2]	HIS 132 [NE2]	ECL1			67					
TYR 11 [OH]	TYR 11 [HH]	SER 214 [OG]	ECL2-β1		51			14			
TYR 11 [OH]	TYR 11 [HH]	SER 214 [N]	ECL2-β1	11	52			11			
TYR 11 [OH]	SER 214 [H]	SER 214 [N]	ECL2-β1	12	74			84			12
TYR 11 [O]	THR 226 [HG1]	THR 226 [OG1]	ECL2-β2	98	100	83	88	98			62
TYR 11 [O]	TYR 347 [HH]	TYR 347 [OH]	TM7						81	92	
TYR 11 [N]	TYR 11 [H]	ASP 54 [OD1]	N-term					48		99	
TYR 11 [N]	TYR 11 [H]	ASP 54 [OD2]	N-term					50		99	
TYR 11 [N]	THR 226 [HG1]	THR 226 [OG1]	ECL2-β2				55		53		
ILE 12 [O]	ARG 327 [HH21]	ARG 327 [NH2]	TM6	99				74			
ILE 12 [O]	ARG 327 [HE]	ARG 327 [NE]	TM6	30				41			
ILE 12 [O]	TYR 347 [HH]	TYR 347 [OH]	TM7	91	100	99	100	35	100	100	96
ILE 12 [N]	ILE 12 [H]	ASP 54 [OD1]	N-term								86
ILE 12 [N]	ILE 12 [H]	ASP 54 [OD2]	N-term								90
ILE 12 [N]	ILE 12 [H]	CYS 225 [O]	ECL2-β2						100	96	
ILE 12 [N]	THR 226 [HG1]	THR 226 [OG1]	ECL2-β2	82	82	57		84		29	35
ILE 12 [N]	ILE 12 [H]	THR 226 [N]	ECL2-β2						59	32	
LEU 13 [O]	TYR 146 [HH]	TYR 146 [OH]	TM3	98	99	95	96	94	98	90	37
LEU 13 [O]	TYR 324 [HH]	TYR 324 [OH]	TM6	98	53			87			
LEU 13 [O]	ARG 327 [HH21]	ARG 327 [NH2]	TM6	11	86	82	88	40	96	90	77

LEU 13 [O]	ARG 327 [HH22]	ARG 327 [NH2]	TM6	55			14	13	13		
LEU 13 [O]	ARG 327 [HE]	ARG 327 [NE]	TM6		29	53	39	16	22	68	41
LEU 13 [O]	ARG 328 [HE]	ARG 328 [NE]	TM6			21	14	41	24	61	14
LEU 13 [O]	TYR 351 [HH]	TYR 351 [OH]	TM7		98	94	100		99	98	95
LEU 13 [OXT]	TYR 146 [HH]	TYR 146 [OH]	TM3	98	98	97	95	95	91	96	36
LEU 13 [OXT]	TYR 324 [HH]	TYR 324 [OH]	TM6	98	59			87	11		
LEU 13 [OXT]	ARG 327 [HH21]	ARG 327 [NH2]	TM6	11	89	66	91	36	98	85	58
LEU 13 [OXT]	ARG 327 [HE]	ARG 327 [NE]	TM6		31	33	48	15	66	17	29
LEU 13 [OXT]	ARG 328 [HE]	ARG 328 [NE]	TM6			16	20	33	56	18	11
LEU 13 [OXT]	TYR 351 [HH]	TYR 351 [OH]	TM7		97	95	100		100	99	95
LEU 13 [N]	LEU 13 [H]	TYR 146 [OH]	TM3	71	76	99	97	46	99	74	11
LEU 13 [N]	TYR 146 [HH]	TYR 146 [OH]	TM3	73	76	100	97	51	95	78	14
LEU 13 [N]	LEU 13 [H]	CYS 225 [O]	ECL2-β2	23				39		60	14
LEU 13 [N]	ARG 327 [HH21]	ARG 327 [NH2]	TM6	90				56			
LEU 13 [N]	TYR 347 [HH]	TYR 347 [OH]	TM7	86	97	98	97		99	93	95
LEU 13 [N]	TYR 351 [HH]	TYR 351 [OH]	TM7		95	89	99				

Table S11. R-factor ratios between theoretical and experimental STD enhancements. Agreement of normalised NT10-13 and NT8-13 STD_{MD} sets with normalised experimental STD and STCD sets assessed via the agreement factor R using equation 7. Also shown are R-factors for the agreement of the crystal structure (PDB 4BUO) STD set the averaged STD_{MD} sets (MD average; considering all 10 MD cluster frames) and the STD_{MD} sets derived from individual MD cluster frames. R-factor ratios are based on the assignments used in the manuscript whereby resonances not stereospecifically assigned were set as used throughout the manuscript: 2.94 ppm Y11 $H^{\beta 2}$, 2.86 ppm Y11 $H^{\beta 3}$, 1.95 ppm P10 $H^{\gamma 2}$, 1.89 ppm P10 $H^{\beta 3}/H^{\gamma 3}$ and 0.83 ppm L13 $H^{\delta 1}$.

	4BUO	MD	MD cluster frame									
		average	1	2	3	4	5	6	7	8	9	10
NT10-13												
STD	0.84	1.08	0.65	1.04	1.11	1.26	1.24	1.28	0.55	1.51	0.71	0.92
STCD	0.74	0.85	0.40	0.79	0.92	0.99	1.05	1.06	0.43	1.23	0.55	0.76
4BUO	-	0.38	0.47	0.44	0.46	0.49	0.41	0.5	0.38	0.74	0.36	0.36
Y11 χ_1	g^+	-	g^-	g^+	g^+	g^-	g^-	g^+	g^+	g^-	g^-	g^-
NT8-13												
STD	0.84	0.90	0.97	0.94	0.55	1.07	1.35	1.30	0.94	1.07	0.41	0.59
STCD	0.74	0.74	0.82	0.65	0.49	0.88	1.11	1.15	0.87	0.88	0.46	0.47
4BUO	-	0.23	0.26	0.46	0.32	0.35	0.54	0.56	0.47	0.47	0.37	0.35
Y11 χ_1	g^+	-	g^+	g^+	g^-	g^+	g^-	g^-	g^-	g^-	g^+	g^-

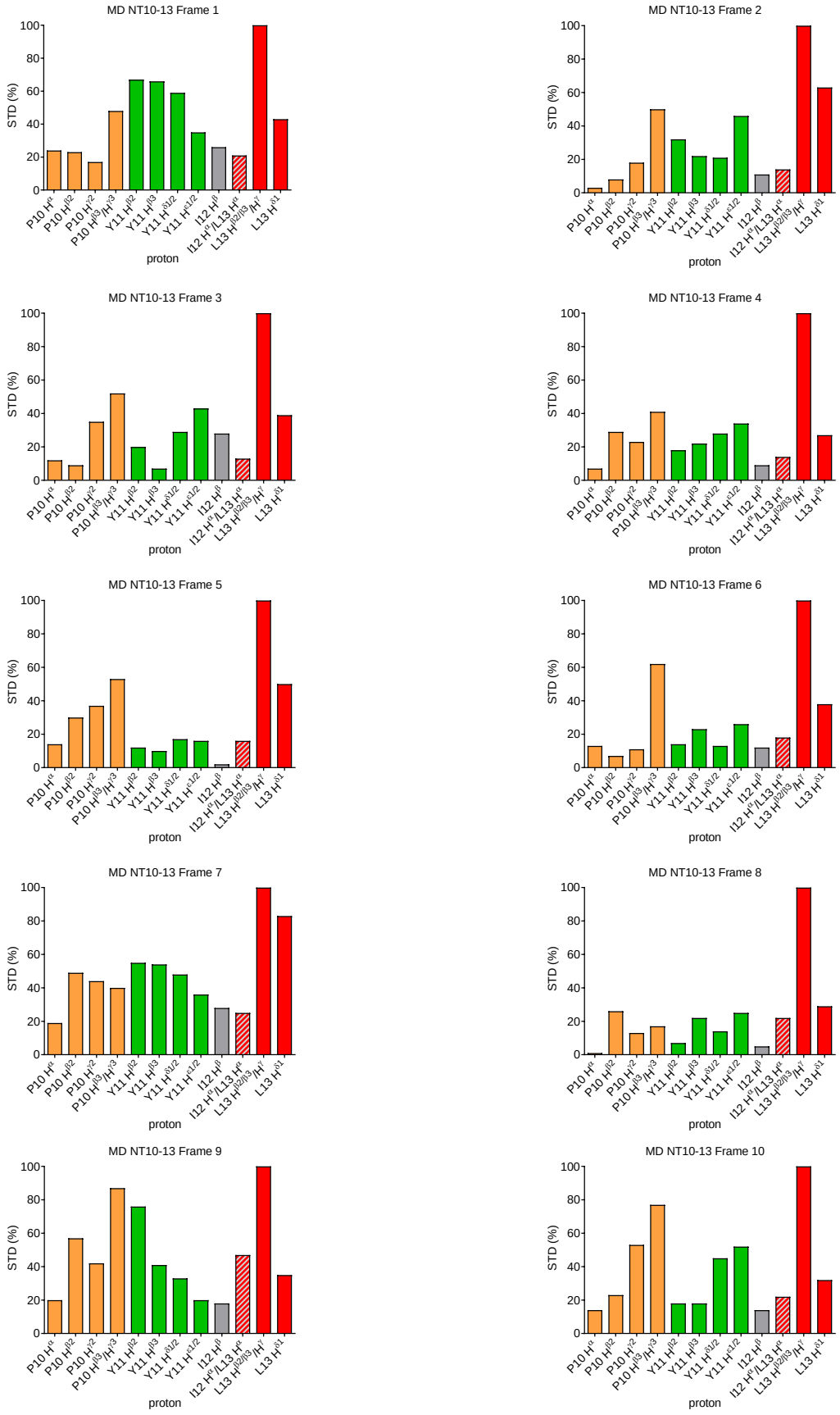

Figure S8. Epitope maps based on theoretical STD enhancements (STD_{MD}) of individual NT10-13 cluster representatives. STD_{MD} values of each set were normalized to the maximum value observed for the respective cluster frame.

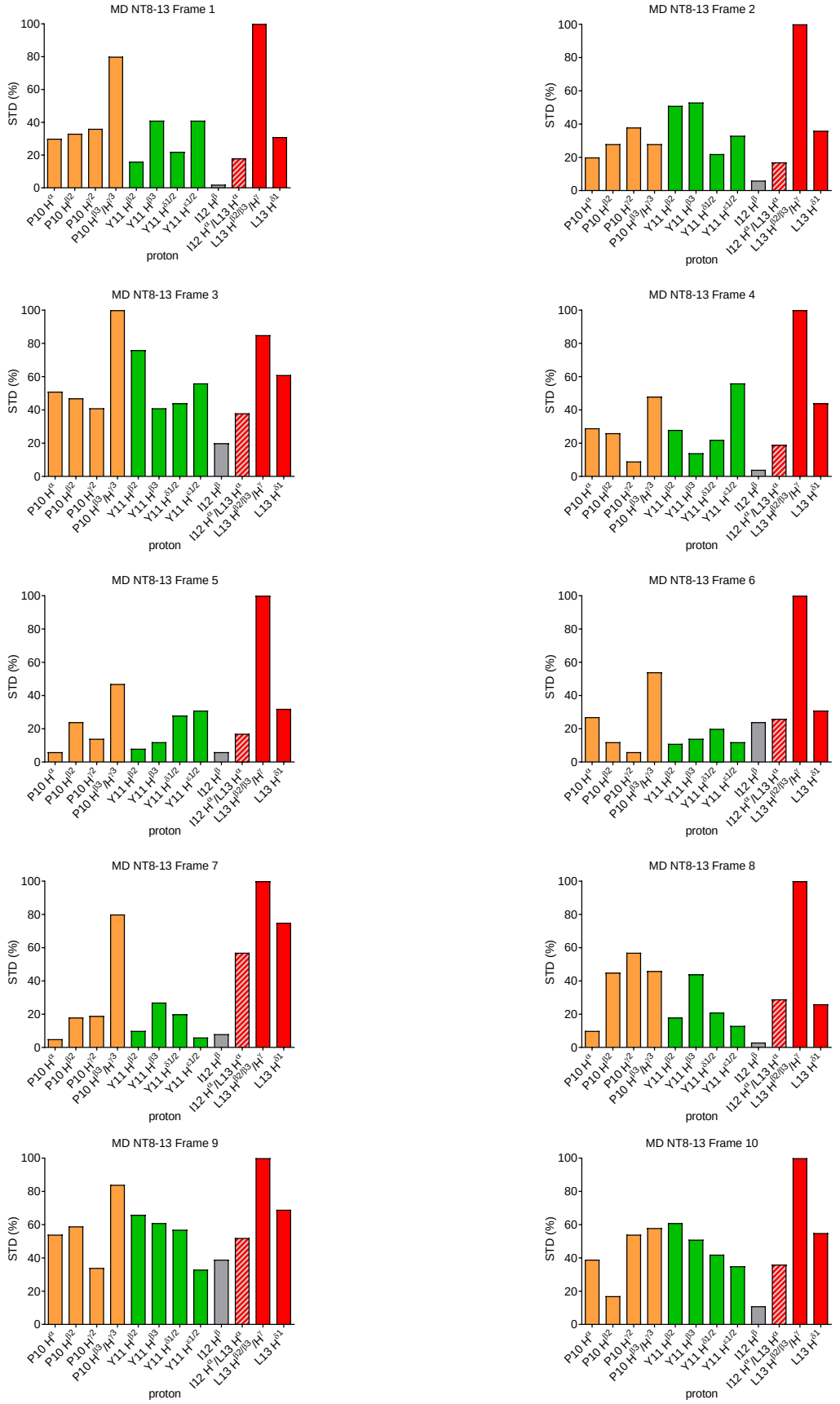

Figure S9. Epitope maps based on theoretical STD enhancements (STD_{MD}) of individual NT8-13 cluster representatives. STD_{MD} values of each set were normalized to the maximum value observed for the respective cluster frame.

Table S12. R-factor ratios between theoretical and experimental STD enhancements assuming alternative assignments. Agreement of normalised NT10-13 and NT8-13 STD_{MD} sets with normalised experimental STD and STCD sets as described in Table S11 but with alternative resonance assignments. The first column shows the alternative assignments used for resonances at 2.94 ppm, 2.86 ppm, 1.95 ppm, 1.89 ppm and 0.83 ppm.

Assignments		4BUO	MD	MD cluster frame									
			average	1	2	3	4	5	6	7	8	9	10
NT10-13													
Y11 $H^{\beta2}$, Y11 $H^{\beta3}$, P10 $H^{\beta3}$, P10 $H^{\gamma2}$/$H^{\gamma3}$, L13 $H^{\delta1}$	STD	0.85	1.08	0.65	1.03	1.11	1.26	1.23	1.28	0.58	1.51	0.72	1.11
	STCD	0.75	0.85	0.40	0.79	0.92	0.99	1.05	1.06	0.46	1.23	0.56	0.92
Y11 $H^{\beta2}$, Y11 $H^{\beta3}$, P10 $H^{\beta3}$, P10 $H^{\gamma2}$/$H^{\gamma3}$, L13 $H^{\delta2}$	STD	0.89	1.09	0.58	1.14	1.04	1.26	1.29	1.28	0.66	1.54	0.73	1.12
	STCD	0.77	0.86	0.37	0.85	0.88	0.99	1.10	1.06	0.48	1.25	0.57	0.93
Y11 $H^{\beta2}$, Y11 $H^{\beta3}$, P10 $H^{\gamma2}$, P10 $H^{\beta3}$/$H^{\gamma3}$, L13 $H^{\delta1}$	STD	0.84	1.08	0.65	1.04	1.11	1.26	1.24	1.28	0.55	1.51	0.71	0.92
	STCD	0.74	0.85	0.40	0.79	0.92	0.99	1.05	1.06	0.43	1.23	0.55	0.76
Y11 $H^{\beta2}$, Y11 $H^{\beta3}$, P10 $H^{\gamma2}$, P10 $H^{\beta3}$/$H^{\gamma3}$, L13 $H^{\delta2}$	STD	0.89	1.09	0.58	1.15	1.04	1.26	1.31	1.28	0.63	1.54	0.72	0.93
	STCD	0.77	0.86	0.37	0.86	0.88	0.99	1.10	1.06	0.45	1.26	0.56	0.77
Y11 $H^{\beta2}$, Y11 $H^{\beta3}$, P10 $H^{\gamma3}$, P10 $H^{\beta3}$/$H^{\gamma2}$, L13 $H^{\delta1}$	STD	0.83	1.08	0.64	1.04	1.11	1.26	1.24	1.28	0.58	1.51	0.69	0.91
	STCD	0.73	0.85	0.38	0.80	0.93	0.99	1.05	1.06	0.45	1.23	0.53	0.76
Y11 $H^{\beta2}$, Y11 $H^{\beta3}$, P10 $H^{\gamma3}$, P10 $H^{\beta3}$/$H^{\gamma2}$, L13 $H^{\delta2}$	STD	0.83	1.09	0.56	1.15	1.05	1.26	1.31	1.28	0.65	1.54	0.70	0.93
	STCD	0.73	0.85	0.35	0.86	0.89	0.99	1.10	1.06	0.47	1.25	0.54	0.77
Y11 $H^{\beta2}$, Y11 $H^{\beta3}$, P10 $H^{\gamma2/\gamma3}$, P10 $H^{\beta3}$, L13 $H^{\delta1}$	STD	0.82	1.07	0.63	1.04	1.10	1.25	1.20	1.26	0.56	1.50	0.69	1.07
	STCD	0.74	0.85	0.40	0.79	0.92	0.99	1.05	1.05	0.45	1.23	0.56	0.91
Y11 $H^{\beta2}$, Y11 $H^{\beta3}$, P10 $H^{\gamma2/\gamma3}$, P10 $H^{\beta3}$, L13 $H^{\delta2}$	STD	0.87	1.08	0.56	1.15	1.04	1.25	1.27	1.27	0.63	1.53	0.70	1.09
	STCD	0.77	0.86	0.37	0.85	0.88	0.99	1.09	1.06	0.47	1.25	0.57	0.93
Y11 $H^{\beta3}$, Y11 $H^{\beta2}$, P10 $H^{\beta3}$, P10 $H^{\gamma2}$/$H^{\gamma3}$, L13 $H^{\delta1}$	STD	0.84	1.09	0.65	1.02	1.10	1.27	1.23	1.29	0.58	1.52	0.70	1.11
	STCD	0.75	0.85	0.40	0.80	0.93	0.99	1.05	1.05	0.46	1.22	0.59	0.92
Y11 $H^{\beta3}$, Y11 $H^{\beta2}$, P10 $H^{\beta3}$, P10 $H^{\gamma2}$/$H^{\gamma3}$, L13 $H^{\delta2}$	STD	0.89	1.10	0.58	1.13	1.03	1.26	1.29	1.29	0.66	1.55	0.71	1.12
	STCD	0.78	0.86	0.37	0.86	0.89	0.99	1.10	1.05	0.48	1.24	0.60	0.93
Y11 $H^{\beta3}$, Y11 $H^{\beta2}$, P10 $H^{\gamma2}$, P10 $H^{\beta3}$/$H^{\gamma3}$, L13 $H^{\delta1}$	STD	0.83	1.08	0.65	1.03	1.10	1.27	1.23	1.28	0.55	1.52	0.69	0.91
	STCD	0.74	0.85	0.40	0.80	0.93	0.99	1.05	1.05	0.43	1.22	0.58	0.76
Y11 $H^{\beta3}$, Y11 $H^{\beta2}$, P10 $H^{\gamma2}$, P10 $H^{\beta3}$/$H^{\gamma3}$, L13 $H^{\delta2}$	STD	0.88	1.09	0.58	1.14	1.04	1.27	1.31	1.28	0.63	1.55	0.70	0.93
	STCD	0.77	0.85	0.37	0.87	0.89	0.99	1.10	1.05	0.45	1.24	0.58	0.77
Y11 $H^{\beta3}$, Y11 $H^{\beta2}$, P10 $H^{\gamma3}$, P10 $H^{\beta3}$/$H^{\gamma2}$, L13 $H^{\delta1}$	STD	0.82	1.08	0.63	1.04	1.10	1.27	1.23	1.28	0.58	1.52	0.67	0.91
	STCD	0.74	0.85	0.39	0.81	0.94	0.99	1.05	1.05	0.46	1.22	0.56	0.76
Y11 $H^{\beta3}$, Y11 $H^{\beta2}$, P10 $H^{\gamma3}$, P10 $H^{\beta3}$/$H^{\gamma2}$, L13 $H^{\delta2}$	STD	0.82	1.09	0.56	1.14	1.04	1.27	1.31	1.29	0.65	1.55	0.68	0.93
	STCD	0.74	0.85	0.35	0.87	0.90	0.99	1.10	1.05	0.47	1.24	0.57	0.77
Y11 $H^{\beta3}$, Y11 $H^{\beta2}$, P10 $H^{\gamma2/\gamma3}$, P10 $H^{\beta3}$, L13 $H^{\delta1}$	STD	0.82	1.07	0.63	1.03	1.09	1.25	1.20	1.27	0.56	1.51	0.67	1.07
	STCD	0.75	0.85	0.40	0.80	0.93	0.99	1.05	1.05	0.46	1.22	0.59	0.91
	STD	0.86	1.08	0.56	1.14	1.03	1.25	1.27	1.27	0.63	1.54	0.68	1.09

Y11 $H^{\beta3}$, Y11 $H^{\beta2}$, P10 $H^{\gamma2/\gamma3}$, P10 $H^{\beta3}$, L13 $H^{\delta2}$	STCD	0.78	0.85	0.37	0.86	0.89	0.99	1.09	1.05	0.47	1.24	0.59	0.93
NT8-13													
Y11 $H^{\beta2}$, Y11 $H^{\beta3}$, P10 $H^{\beta3}$, P10 $H^{\gamma2}/H^{\gamma3}$, L13 $H^{\delta1}$	STD	0.85	0.90	0.97	0.96	0.41	1.06	1.35	1.31	0.93	1.08	0.44	0.65
	STCD	0.75	0.75	0.81	0.67	0.43	0.87	1.11	1.16	0.86	0.89	0.48	0.53
Y11 $H^{\beta2}$, Y11 $H^{\beta3}$, P10 $H^{\beta3}$, P10 $H^{\gamma2}/H^{\gamma3}$, L13 $H^{\delta2}$	STD	0.90	0.91	0.97	0.91	0.46	1.10	1.29	1.34	0.99	1.03	0.44	0.67
	STCD	0.77	0.75	0.82	0.64	0.44	0.89	1.07	1.18	0.90	0.86	0.48	0.54
Y11 $H^{\beta2}$, Y11 $H^{\beta3}$, P10 $H^{\gamma2}$, P10 $H^{\beta3}/H^{\gamma3}$, L13 $H^{\delta1}$	STD	0.84	0.90	0.97	0.94	0.55	1.07	1.35	1.30	0.94	1.07	0.41	0.59
	STCD	0.74	0.74	0.82	0.65	0.49	0.88	1.11	1.15	0.87	0.88	0.46	0.47
Y11 $H^{\beta2}$, Y11 $H^{\beta3}$, P10 $H^{\gamma2}$, P10 $H^{\beta3}/H^{\gamma3}$, L13 $H^{\delta2}$	STD	0.89	0.90	0.97	0.89	0.60	1.10	1.29	1.33	1.00	1.02	0.41	0.61
	STCD	0.77	0.74	0.82	0.62	0.51	0.90	1.07	1.17	0.90	0.84	0.46	0.48
Y11 $H^{\beta2}$, Y11 $H^{\beta3}$, P10 $H^{\gamma3}$, P10 $H^{\beta3}/H^{\gamma2}$, L13 $H^{\delta1}$	STD	0.82	0.89	0.95	0.94	0.55	1.06	1.34	1.31	0.92	1.06	0.37	0.59
	STCD	0.73	0.74	0.82	0.66	0.50	0.87	1.11	1.16	0.86	0.88	0.43	0.48
Y11 $H^{\beta2}$, Y11 $H^{\beta3}$, P10 $H^{\gamma3}$, P10 $H^{\beta3}/H^{\gamma2}$, L13 $H^{\delta2}$	STD	0.88	0.83	0.97	0.91	0.64	1.09	1.29	1.33	0.98	1.03	0.36	0.63
	STCD	0.76	0.74	0.82	0.63	0.53	0.89	1.07	1.18	0.90	0.85	0.43	0.49
Y11 $H^{\beta2}$, Y11 $H^{\beta3}$, P10 $H^{\gamma2/\gamma3}$, P10 $H^{\beta3}$, L13 $H^{\delta1}$	STD	0.82	0.88	0.96	0.94	0.41	1.06	1.35	1.30	0.91	1.05	0.40	0.61
	STCD	0.74	0.74	0.81	0.67	0.43	0.87	1.11	1.16	0.86	0.89	0.48	0.53
Y11 $H^{\beta2}$, Y11 $H^{\beta3}$, P10 $H^{\gamma2/\gamma3}$, P10 $H^{\beta3}$, L13 $H^{\delta2}$	STD	0.87	0.89	0.96	0.89	0.45	1.09	1.29	1.32	0.97	1.00	0.40	0.63
	STCD	0.77	0.75	0.81	0.64	0.44	0.89	1.07	1.18	0.90	0.86	0.48	0.54
Y11 $H^{\beta3}$, Y11 $H^{\beta2}$, P10 $H^{\beta3}$, P10 $H^{\gamma2}/H^{\gamma3}$, L13 $H^{\delta1}$	STD	0.84	0.91	0.99	0.96	0.39	1.05	1.35	1.31	0.94	1.09	0.44	0.64
	STCD	0.75	0.74	0.80	0.67	0.45	0.88	1.10	1.16	0.85	0.87	0.48	0.54
Y11 $H^{\beta3}$, Y11 $H^{\beta2}$, P10 $H^{\beta3}$, P10 $H^{\gamma2}/H^{\gamma3}$, L13 $H^{\delta2}$	STD	0.89	0.91	0.99	0.91	0.44	1.09	1.30	1.34	1.00	1.05	0.43	0.66
	STCD	0.78	0.75	0.80	0.64	0.47	0.90	1.06	1.18	0.89	0.84	0.48	0.55
Y11 $H^{\beta3}$, Y11 $H^{\beta2}$, P10 $H^{\gamma2}$, P10 $H^{\beta3}/H^{\gamma3}$, L13 $H^{\delta1}$	STD	0.83	0.90	0.99	0.94	0.53	1.06	1.35	1.30	0.95	1.09	0.41	0.58
	STCD	0.74	0.74	0.80	0.65	0.51	0.89	1.10	1.15	0.86	0.86	0.46	0.48
Y11 $H^{\beta3}$, Y11 $H^{\beta2}$, P10 $H^{\gamma2}$, P10 $H^{\beta3}/H^{\gamma3}$, L13 $H^{\delta2}$	STD	0.88	0.90	0.99	0.89	0.58	1.09	1.29	1.33	1.01	1.03	0.40	0.61
	STCD	0.77	0.74	0.80	0.62	0.54	0.91	1.06	1.17	0.89	0.82	0.46	0.49
Y11 $H^{\beta3}$, Y11 $H^{\beta2}$, P10 $H^{\gamma3}$, P10 $H^{\beta3}/H^{\gamma2}$, L13 $H^{\delta1}$	STD	0.82	0.89	0.97	0.94	0.53	1.05	1.34	1.31	0.93	1.07	0.36	0.58
	STCD	0.74	0.73	0.80	0.66	0.53	0.88	1.10	1.16	0.85	0.86	0.44	0.49
Y11 $H^{\beta3}$, Y11 $H^{\beta2}$, P10 $H^{\gamma3}$, P10 $H^{\beta3}/H^{\gamma2}$, L13 $H^{\delta2}$	STD	0.87	0.91	0.99	0.91	0.62	1.09	1.30	1.33	0.99	1.04	0.36	0.62
	STCD	0.77	0.74	0.80	0.63	0.56	0.90	1.06	1.18	0.88	0.83	0.44	0.50
Y11 $H^{\beta3}$, Y11 $H^{\beta2}$, P10 $H^{\gamma2/\gamma3}$, P10 $H^{\beta3}$, L13 $H^{\delta1}$	STD	0.82	0.89	0.97	0.94	0.38	1.05	1.35	1.30	0.92	1.07	0.40	0.61
	STCD	0.75	0.74	0.79	0.67	0.45	0.88	1.10	1.16	0.85	0.87	0.48	0.53
Y11 $H^{\beta3}$, Y11 $H^{\beta2}$, P10 $H^{\gamma2/\gamma3}$, P10 $H^{\beta3}$, L13 $H^{\delta2}$	STD	0.87	0.89	0.97	0.89	0.43	1.08	1.29	1.33	0.98	1.02	0.39	0.63
	STCD	0.78	0.74	0.79	0.64	0.47	0.90	1.06	1.18	0.88	0.84	0.48	0.54

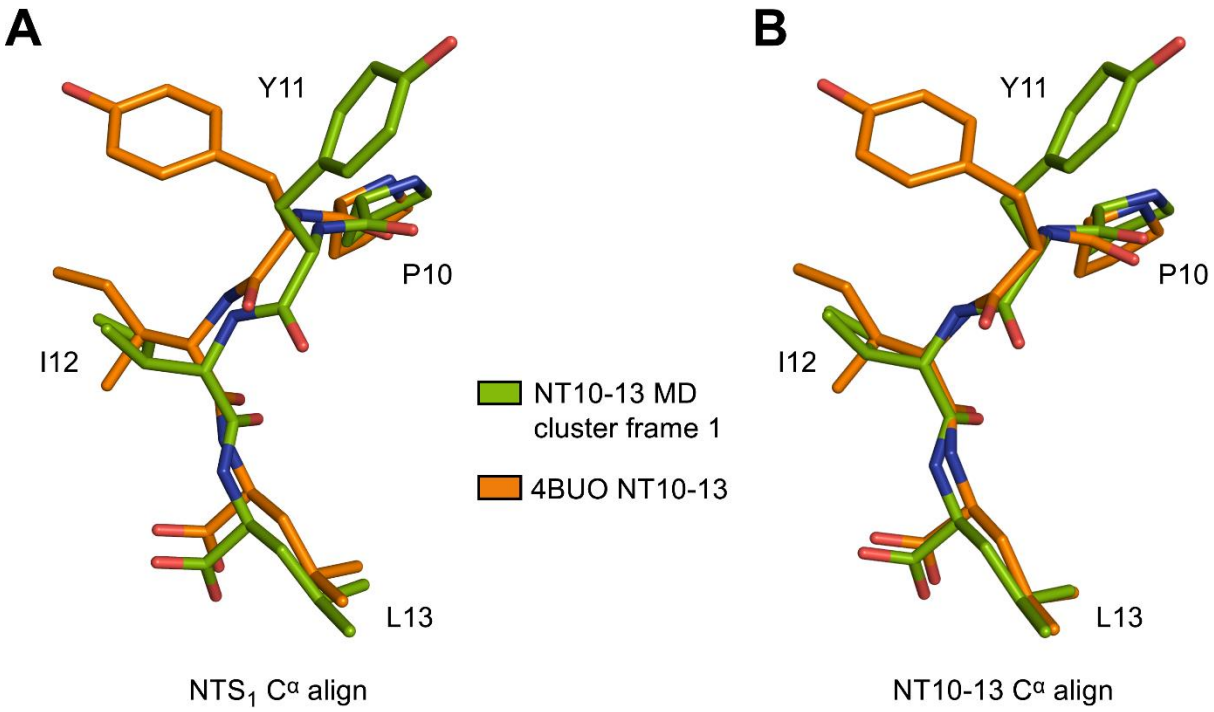

Figure S10. Comparison of NT10-13 in MD cluster frame 1 and PDB 4BUO. Superimpositions of exposed views of NT10-13 as observed in MD cluster frame 1 (green) and the crystal structure (PDB 4BUO, orange). Residues R8 and R9 of the PDB 4BUO peptide were omitted for simplicity. A) Alignment based on C^{α} atoms of the whole NTS_1-peptide complex showing relative orientation of the two peptides to each other. B) Alignment based on C^{α} atoms of only NT10-13 residues revealing similar backbone conformations of the two peptides (RMSD = 0.246 Å).

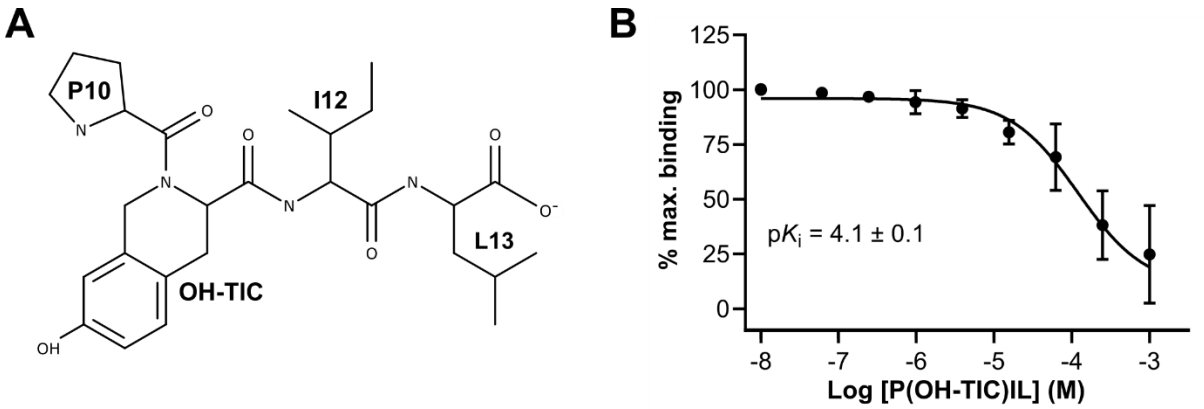

Figure S11. Conformationally restrained P(OH-TIC) peptide. A) Structure of P(OH-TIC)IL with the sidechains labelled as they are referred to in the text. B) Inhibition of TAMRA-NT8-13 binding to MBP-enNTS$_1$-muGFP using varying concentrations of P(OH-TIC)IL. Values reported represent the mean and standard deviation (SD) of three independent triplicates (n = 3) of the TAMRA fluorescence to muGFP ratio calculated for each measurement, plotted against P(OH-TIC)IL concentration. The -log dissociation constant (pKi) of P(OH-TIC)IL is reported with the standard error (SE) calculated from each experiment.

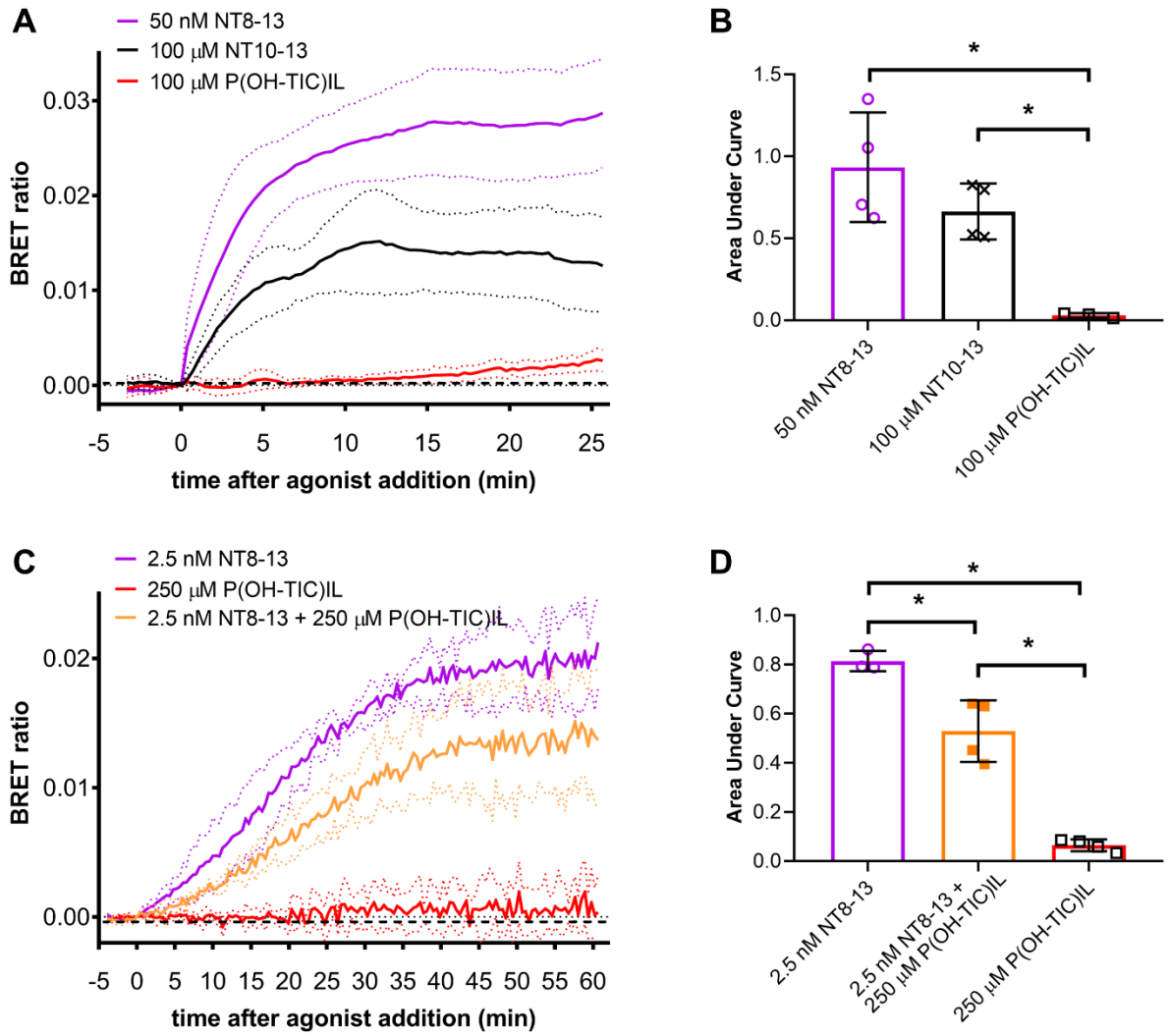

Figure S12. P(OH-TIC)IL does not stimulate recruitment of human β-arrestin 2 to hNTS$_1$. NanoBRET assay using HEK 293T cells transfected with a WT hNTS$_1$-NanoLuc fusion and hβ-arrestin 2-Venus fusion. Luminescence emission at two wavelengths (donor and acceptor) were measured simultaneously every 30-40 seconds before and after ligand addition (at time 0). Mean ligand stimulated changes in BRET ratio (pooled over three or four individual experiments) are presented in A) and C) with the dotted lines indicating the standard deviation (SD) at each timepoint. B) The area under the individual replicate experiment curves (i.e. from A)) are plotted as points and bars (± SD.) D) The area under the individual replicate experiment curves (i.e. from C)) are plotted as points and bars (± SD).* represents statistically significant differences (One-Way ANOVA with Tukey multiple comparisons test)

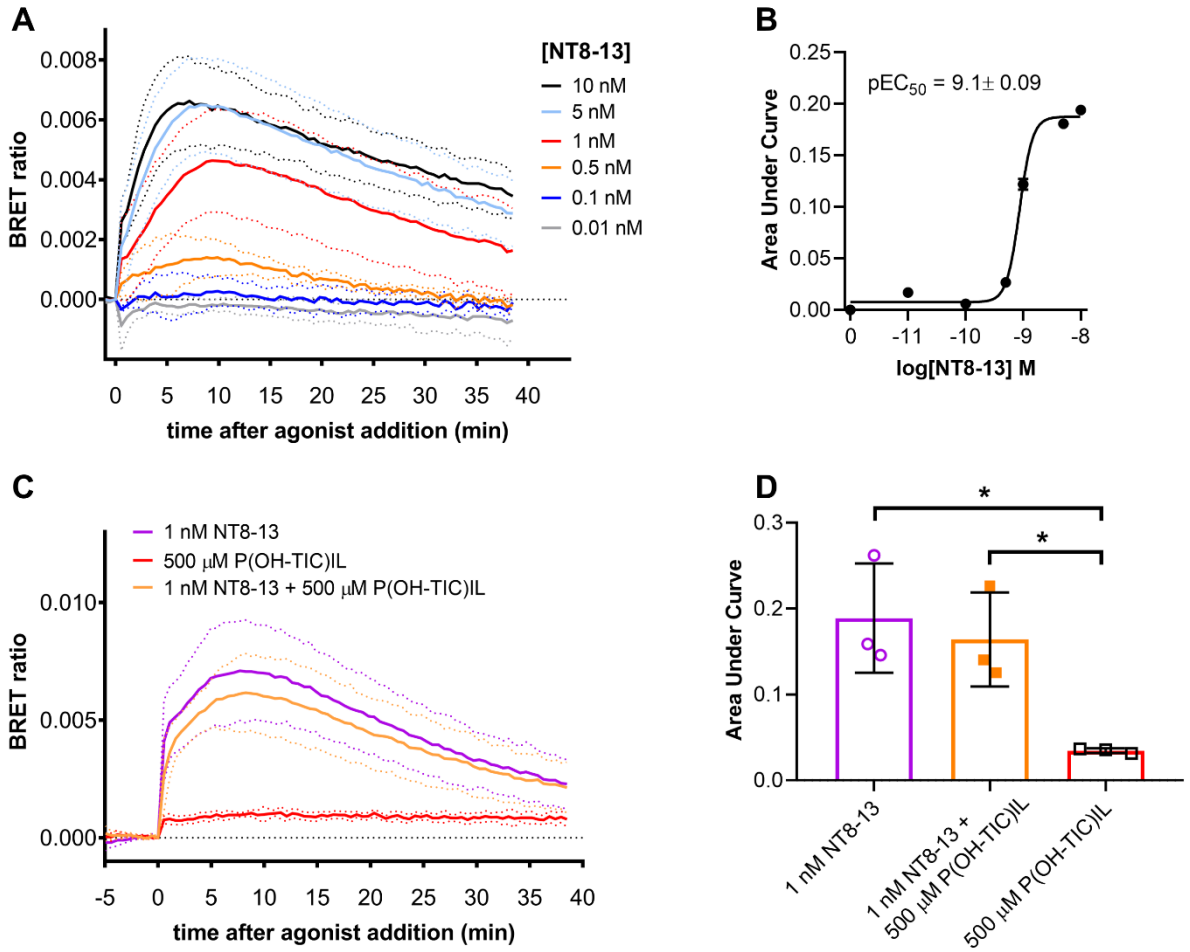

Figure S13. P(OH-TIC)IL does not antagonise NT8-13 Gβγ release from hNTS$_1$. NanoBRET assay using HEK 293T cells transfected with a WT hNTS$_1$, Gαq, a Gβ/γ split-Venus fusion and masGRK3 C-terminus fused to NanoLuc (masGRK3CT-NanoLuc). Luminescence emission at two wavelengths (donor and acceptor) were measured simultaneously measured every 30-40 seconds before and after ligand addition (at time 0). Mean ligand stimulated changes in BRET ratio (pooled over three experiments) are presented in A) and C) with the dotted lines indicating the standard deviation (SD) at each timepoint. B) Dose response curve of NT8-13 stimulating Gβ/γ-Venus interaction with masGRK3CT-NanoLuc (BRET). Data points are the area under the curve measurements from replicate experiments in A). The pEC$_{50}$ of NT8-13 was calculated in Graphpad Prism and is in agreement with other assays, thus indicating that this NanoBRET assays is a robust measure of NTS$_1$ G protein activation. D) The areas under the individual replicate experiment curves (i.e. from C)) are plotted as points and bars (± SD).* represents statistically significant differences (One-Way ANOVA with Tukey multiple comparisons test)

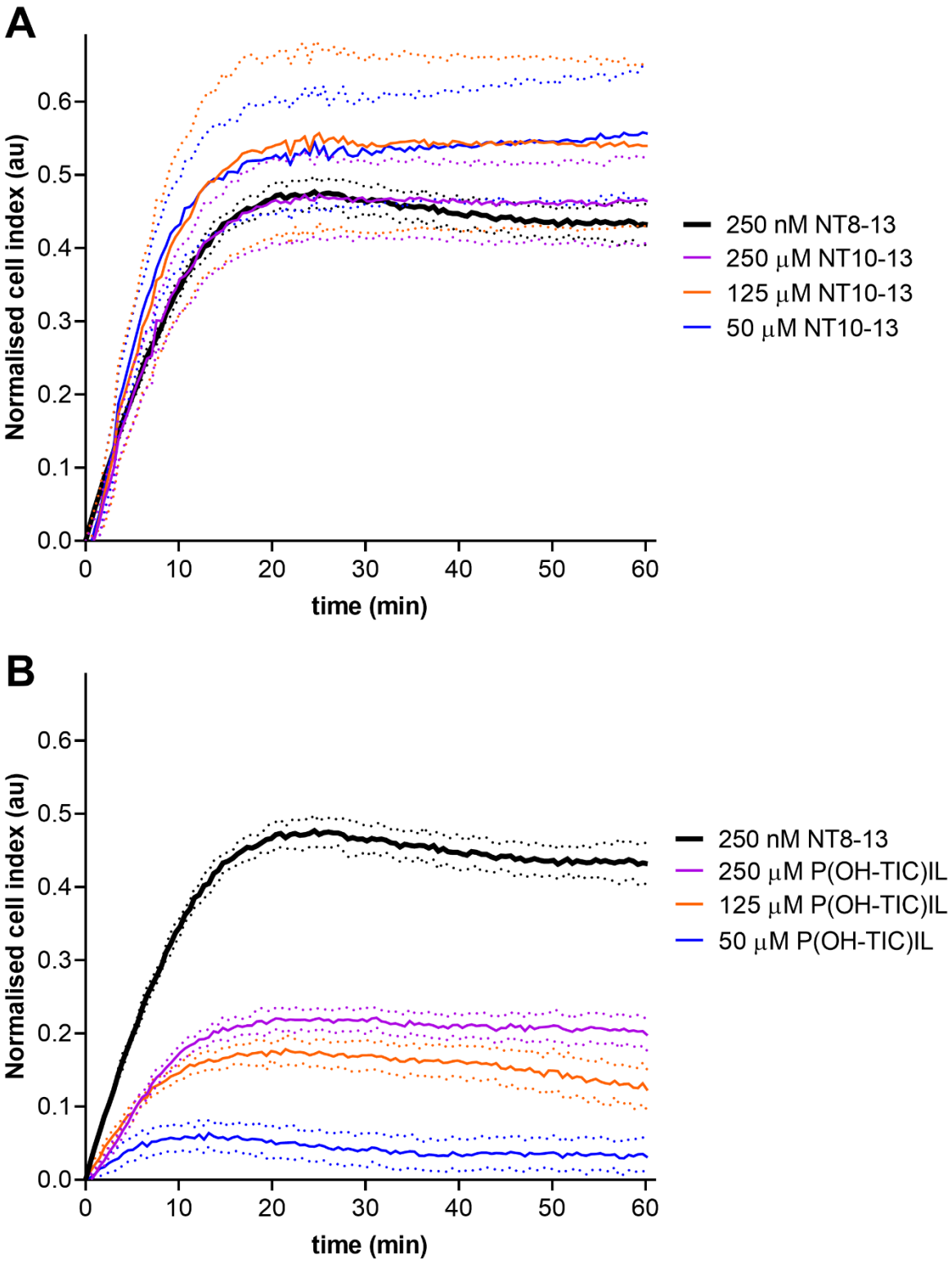

Figure S14. Representative xCELLigence cell index traces after 250 nM NT8-13 treatment (solid black lines in A) and B)), different concentrations of NT10-13 in A) and different P(OH-TIC)IL concentrations in B). Traces represent the mean normalised CI values from three replicate readings (± SD, dotted lines). Replicate curves such as these were used to calculate the area under the curve data in Figure 5E.

Supporting Information

The effect of frequency offset for selective saturation

The frequency for selective (on-resonance) saturation of receptor resonances in STD-NMR experiments corresponding to the spectra shown above was set to -1 ppm to avoid direct excitation of either ligand or detergent resonances. The excitation bandwidth (Δf in Hz) of a pulse is defined as the frequency window over which the pulse is 70% effective and can be determined using the equation[9]:

$$\Delta f = \frac{F}{\Delta t}$$

where F is the shape-specific bandwidth factor and Δt the duration of the pulse. For a 50 ms (Δt) Gaussian pulse, F is 2.1 and therefore Δf is 42 Hz (0.06 ppm at 700 MHz). Hence, a 50 ms Gaussian pulse is 70% effective at ± 0.03 ppm from the saturation frequency while less efficient sidebands will be observable. Selective excitation was tested at 0, -0.5, -1 and -2 ppm using radio frequency field strengths (ω_{RF}) of 86 Hz and 192 Hz (Figure S15). Set at -1 ppm, the pulse appears sufficiently far away from the most upfield NT10-13 resonance observed at 0.76 ppm as well as DDM resonances observed at 0.6 ppm, while a 192 Hz power level brought the saturation close to efficiencies observed at 0 ppm/86 Hz. Selective excitation at 0 ppm and -0.5 ppm, however, resulted in direct excitation of NT10-13 while -2 ppm was inefficient at both power levels. To move the selective excitation offset far away from both peptide methyl and detergent signals we also explored downfield excitation frequencies. Although the most down field NT10-13 resonance was observed at 8.06 ppm, 10 ppm was found to directly saturate the peptide, manifested as a significant enhancement of the L13 H^N (7.69 ppm) but also the Y11 $H^{\delta1/\delta2}$ (7.06 ppm) and Y11 $H^{\varepsilon1/\varepsilon2}$ (6.77 ppm) resonances when looking at a mixture of only NT10-13 in buffer containing DDM (Figure S16B). Moving the selective saturation further downfield to 11 ppm reduced but did not solve the problem of direct saturation of the peptide. Even at 11 ppm selective saturation enhancement of DDM signals is observed. However, this could also be a result of the peptide interacting with the detergent leading to cross relaxation from the saturated peptide to the detergent. In the presence of cleaved enNTS$_1$ the STD effect for certain protons (e.g. P10 H^{α} at 4.20 ppm), was weak at 11 ppm selective saturation, but clearly observable at 10 ppm selective saturation (Figure S16A). As residual STD effects seem to bleed-through regardless of excitation frequency raised the question to what extent those effects are influenced by the detergent. We therefore ran NT10-13-only STD experiments at -1 ppm and 10 ppm selective saturation in buffer without DDM (Figure S17). At at -1 ppm selective saturation the most up field resonances L13 $H^{\delta1}$ at 0.83 ppm, I12 $H^{\gamma2}$ at 0.8 ppm and I12 $H^{\delta2}$ at 0.76 ppm were enhanced despite omitting the DDM indicating that those enhancements are caused by direct saturation of the peptide (black spectrum and up field inset). Enhancement was also observed for L13 $H^{\beta2/\beta3}/H^{\gamma}$ which resonate further downfield at 1.45 ppm. When selectively saturating the DDM free NT10-13 sample at 10 ppm (red spectrum and down field inset) the enhancement of L13 H^N at 7.7 ppm

decreased when compared to the same experiment conducted in presence of DDM (Figure S16B, black trace). For both cases, however, it can be concluded that the resonances at either periphery of the spectrum are affected by direct saturation.

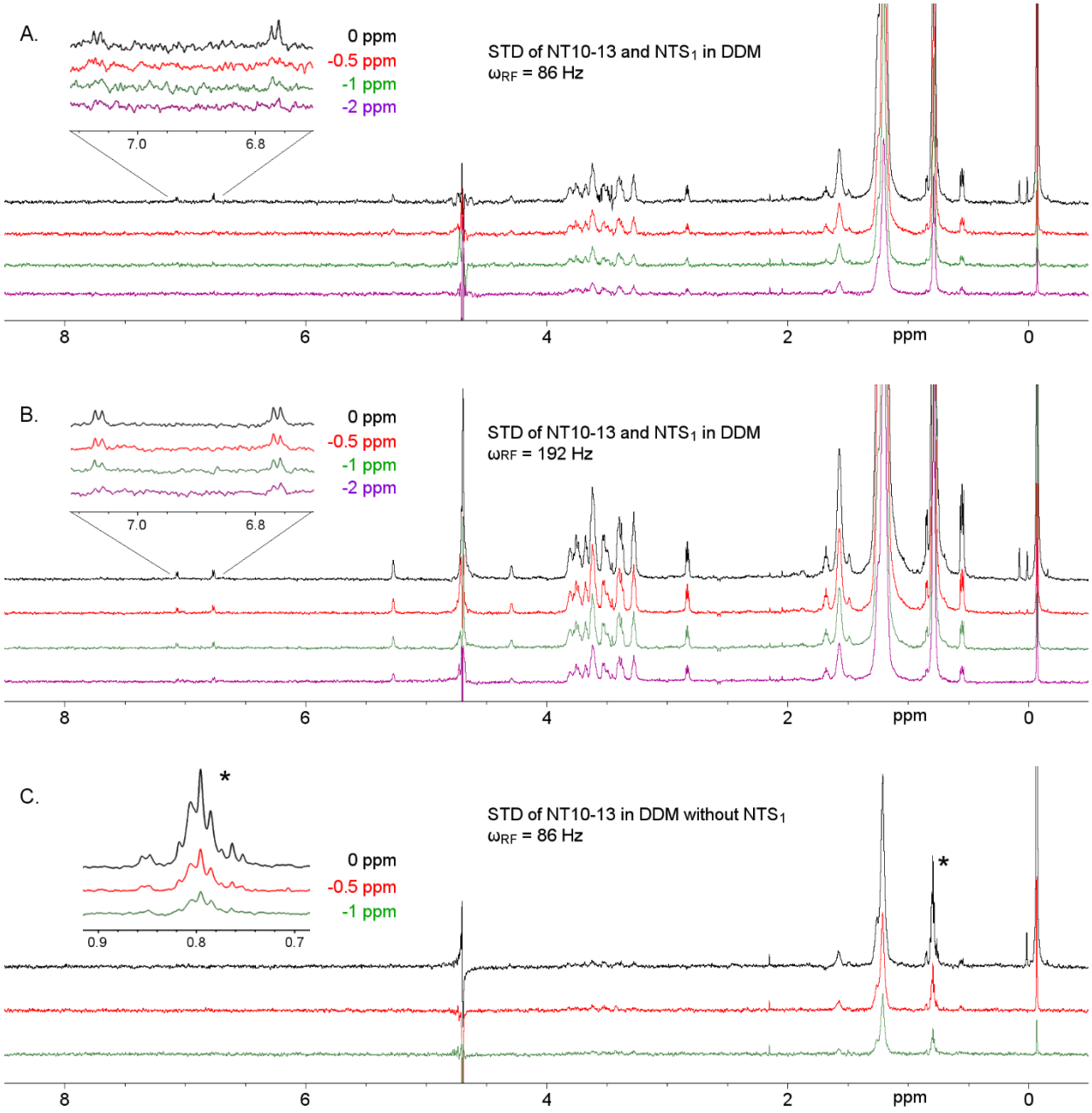

Figure S15. Effects of up field selective excitation pulse offsets and power levels. A) STD spectra recorded using a pulse power level of 86 Hz and selective excitation offsets of 0 ppm (black trace), -0.5 ppm (red trace), -1 ppm (green trace) and -2 ppm (purple trace). B) STD spectra recorded using a pulse power level of 192 Hz and selective excitation offsets of 0 ppm (black trace), -0.5 ppm (red trace), -1 ppm (green trace) and -2 ppm (purple trace). Insets zoom in on Y11 $H^{\delta1/\delta2}$ (7.06 ppm) and Y11 $H^{\varepsilon1/\varepsilon2}$ (6.77 ppm) resonances. Samples A and B both contained 5 µM cleaved enNTS$_1$, 500 µM NT10-13 and 500 µM DSS in buffer: 50 mM Potassium Phosphate, 100 mM NaCl, 1 mM DDM, pH 7.4. C) STD spectra of NT10-13 only showing direct irradiation effect on NT10-13 at selective excitation offsets of 0 ppm (black trace), -0.5 ppm (red trace), -1 ppm (green trace) at a pulse power level of 86 Hz. Inset zooms in on the most up field NT10-13 resonances I12 $H^{\delta2}$ (0.76 ppm), I12 $H^{\gamma2}$/L13 $H^{\delta2}$ (0.8 ppm) and L13 $H^{\delta1}$ (0.83 ppm). Sample C contained 500 µM NT10-13 and 500 µM DSS in buffer: 50 mM potassium phosphate, 100 mM NaCl, 1 mM DDM, pH 7.4.

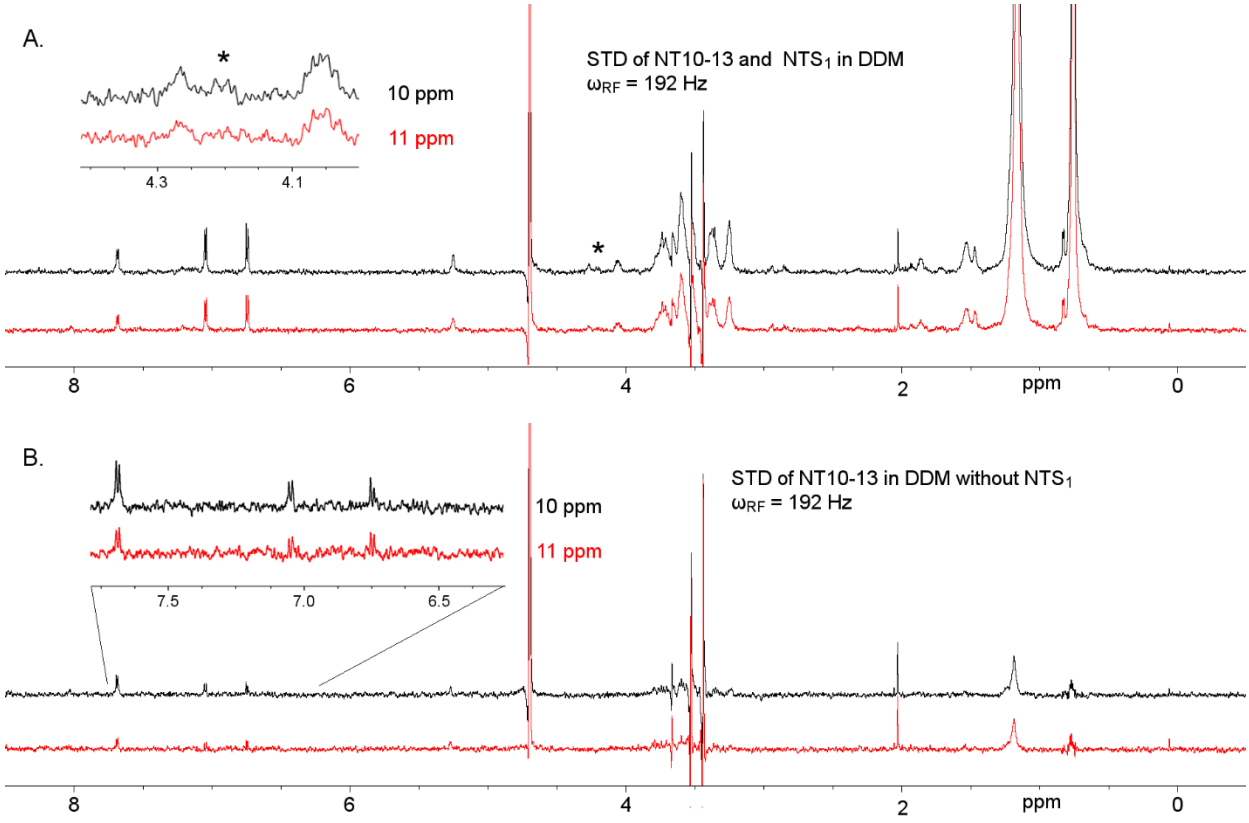

Figure S16. Effects of down field selective excitation pulse offsets. A) STD spectra recorded using selective excitation offsets of 10 ppm (black trace) and 11 ppm (red trace). Inset zooms in on P10 H^{α} (4.2 ppm, marked with a star). Sample A contained 5 µM cleaved enNTS$_1$, 500 µM NT10-13 in buffer: 50 mM Potassium Phosphate, 100 mM NaCl, 400 µM DDM, pH 7.4. B) STD spectra of NT10-13 only showing direct irradiation effect on NT10-13 at selective excitation offsets of 10 ppm (black trace) and 11 ppm (red trace). Inset zooms in on L13 H (7.7 ppm), Y11 $H^{\delta 1/\delta 2}$ (7.06 ppm) and Y11 $H^{\varepsilon 1/\varepsilon 2}$ (6.77 ppm). Sample B contained 500 µM NT10-13 in buffer: 50 mM potassium phosphate, 100 mM NaCl, 400 µM DDM, pH 7.4. The pulse power level was set to 192 Hz in all experiments.

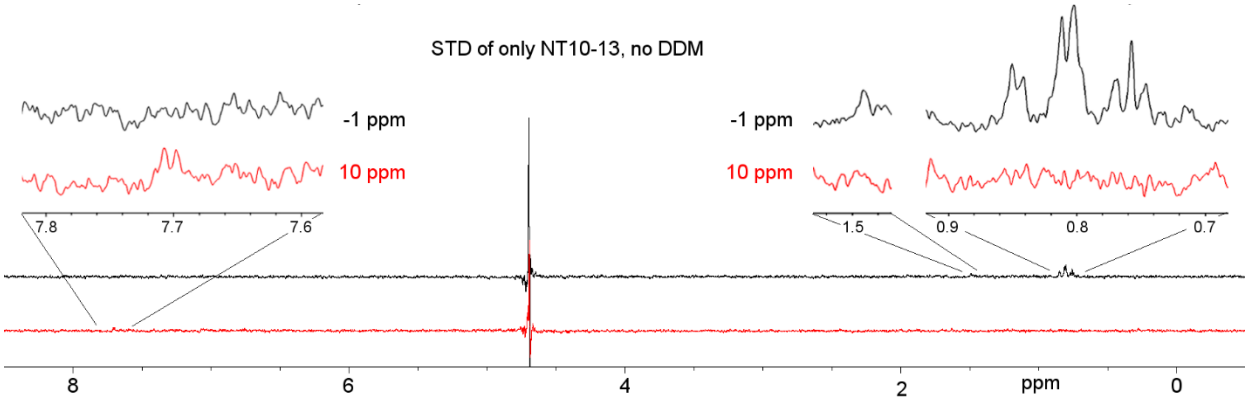

Figure S17. Direct NT10-13 saturation effects of selective excitation pulse offsets at -1 ppm and 10 ppm in the absence of both DDM and enNTS$_1$. STD spectra recorded using selective excitation offsets of -1 ppm (black trace) and 10 ppm (red trace). Down field inset zooms in on L13 H^N (7.7 ppm) and up field insets zoom in on L13 $H^{\beta2/\beta3}/H^{\gamma}$ (1.45 ppm), L13 $H^{\delta1}$ (0.83 ppm), L13 $H^{\delta2}$/I12 $H^{\gamma2}$ (0.8 ppm) and I12 $H^{\delta2}$ (0.76 ppm). The sample contained 500 µM NT10-13 in buffer: 50 mM potassium phosphate, 100 mM NaCl, pH = 7.4. The pulse power level was set to 192 Hz in both experiments.

References

1. Bumbak, F., Keen, A. C., Gunn, N. J., Gooley, P. R., Bathgate, R. A. D., and Scott, D. J. (2018) Optimization and 13CH3 methionine labeling of a signaling competent neurotensin receptor 1 variant for NMR studies, *Biochimica et Biophysica Acta (BBA) - Biomembranes 1860*, 1372-1383.
2. Beauchamp, K. A., Bowman, G. R., Lane, T. J., Maibaum, L., Haque, I. S., and Pande, V. S. (2011) MSMBuilder2: Modeling Conformational Dynamics on the Picosecond to Millisecond Scale, *Journal of Chemical Theory and Computation 7*, 3412-3419.
3. Hartigan, J. A., and Wong, M. A. (1979) Algorithm AS 136: A K-Means Clustering Algorithm, *Journal of the Royal Statistical Society. Series C (Applied Statistics) 28*, 100-108.
4. Vriend, G. (1990) WHAT IF: A molecular modeling and drug design program, *Journal of Molecular Graphics 8*, 52-56.
5. Egloff, P., Hillenbrand, M., Klenk, C., Batyuk, A., Heine, P., Balada, S., Schlinkmann, K. M., Scott, D. J., Schutz, M., and Pluckthun, A. (2014) Structure of signaling-competent neurotensin receptor 1 obtained by directed evolution in Escherichia coli, *Proc Natl Acad Sci U S A 111*, E655-E662.
6. White, J. F., Noinaj, N., Shibata, Y., Love, J., Kloss, B., Xu, F., Gvozdenovic-Jeremic, J., Shah, P., Shiloach, J., Tate, C. G., and Grisshammer, R. (2012) Structure of the agonist-bound neurotensin receptor, *Nature 490*, 508-513.
7. Krumm, B. E., White, J. F., Shah, P., and Grisshammer, R. (2015) Structural prerequisites for G-protein activation by the neurotensin receptor, *Nature communications 6*, 7895.
8. McGibbon, Robert T., Beauchamp, Kyle A., Harrigan, Matthew P., Klein, C., Swails, Jason M., Hernández, Carlos X., Schwantes, Christian R., Wang, L.-P., Lane, Thomas J., and Pande, Vijay S. (2015) MDTraj: A Modern Open Library for the Analysis of Molecular Dynamics Trajectories, *Biophysical Journal 109*, 1528-1532.
9. Claridge, T. D. W. (2016) Chapter 12 - Experimental Methods, In *High-Resolution NMR Techniques in Organic Chemistry (Third Edition)*, pp 457-498, Elsevier, Boston.